Analytical Model to Predict Dilation Behavior of FRP Confined Circular Concrete Columns Subjected to Axial Compressive Loading

Javad Shayanfar [1], Mohammadali Rezazadeh [2] and Joaquim A. Barros [3]

[1] PhD Candidate, ISISE, Department of Civil Engineering, University of Minho, Azurém 4800-058 Guimarães, Portugal, arch3d.ir@gmail.com (corresponding author)

[2] PhD, Civil Eng., ISISE, Department of Civil Engineering, University of Minho, Azurém 4800-058 Guimarães, Portugal, rzh.moh@gmail.com

[3] Full Prof., ISISE, IBS, Department of Civil Engineering, University of Minho, Azurém 4800-058 Guimarães, Portugal, barros@civil.uminho.pt

Abstract:

Experimental research and real case applications are demonstrating that the use of fiber-reinforced polymer (FRP) composite materials can be a solution to substantially improve circular cross-section concrete columns in terms of strength, ductility, and energy dissipation. The present study is dedicated to developing a new model for estimating the dilation behavior of fully and partially FRP-based confined concrete columns under axial compressive loading. By considering experimental observations and results, a new relation between secant Poisson's ratio and axial strain is proposed. In order the model be applicable to partial confinement configurations, a confinement stiffness index is proposed based on the concept of confinement efficiency factor. A new methodology is also developed to predict the ultimate condition of partially FRP confined concrete taking into account the possibility of concrete crushing and FRP rupture failure modes. By comparing the results from experimental tests available in the literature with those determined with the model, the reliability and the good predictive performance of the developed model are demonstrated.

Keywords: FRP confined concrete columns; Full and partial confinement; Dilation behavior; Analytical model; Confinement stiffness index

Notations

A_{eff}	Effectively confined concrete area	V_{con}	Volume of concrete
A_g	Entire concrete area	V_{FRP}	Volume of fibers
c_1	Non-dimensional empirical coefficient	v_s	Secant Poisson's ratio
c_2	Non-dimensional empirical coefficient	$v_{s,0}$	Initial Poisson's ratio of unconfined concrete
c_3	Non-dimensional empirical coefficient	$v_{s,max}$	Maximum Poisson's ratio at the critical section
c_4	Non-dimensional empirical coefficient	$v_{s,u}$	Ultimate Poisson's ratio
D	Diameter of circular column	v'_s	Poisson's ratio at the mid-plane of FRP strips
D'	Width of effective confinement area	$v'_{s,max}$	Maximum Poisson's ratio at strip region
E_f	FRP modulus elasticity	w_f	FRP width
f_c	Axial stress corresponding to ε_c	ε_c	Axial strain corresponding to σ_c
f_f	FRP confining stress of full system	ε_{c0}	Axial strain corresponding to f_{c0}
f_l	FRP confinement pressure of full system	ε_{cc}	Axial strain corresponding to f'_{cc}
$f_{l,i}$	Confinement pressure at the mid-plane of FRP strips	ε_{cu}	Ultimate axial strain
$f_{l,j}$	Confinement pressure at the critical section	$\varepsilon_{cu,r}$	Ultimate axial strain at FRP rupture
f_{c0}	Peak compressive stress of unconfined concrete	$\varepsilon_{cu,c}$	Ultimate axial strain at concrete crushing
f'_{cc}	Peak compressive stress of confined concrete	ε_{fu}	Ultimate FRP tensile strain
f'_f	FRP confining stress of partial system	$\varepsilon_{h.P}$	FRP hoop strain in partial confinement
f'_l	Effective confinement pressure	$\varepsilon_{h,F}$	FRP hoop strain in full confinement
K_e	Confinement efficiency factor = $k_\varepsilon \times k_v$	$\varepsilon_{h,rup}$	FRP hoop rupture strain
k_v	Reduction factor	$\varepsilon_{l,i}$	Concrete expansion at the mid-plane of FRP strips
k_ε	Reduction factor	$\varepsilon_{l,j}$	Lateral concrete expansion at the critical section
n_f	FRP layer number	$\varepsilon_{c,m}$	Axial strain corresponding to $v_{s,max}$
s_f	Distance between FRP strips	ε_v	Volumetric strain
s'	Clear distance between two adjacent steel stirrups	ρ_K	FRP confinement stiffness index
t_f	FRP thickness	$v_{t,eff}$	Effective tangential Poisson's ratio

Introduction

It is well-known that the application of fiber-reinforced polymer (FRP) composites to externally confine concrete columns can lead to substantial enhancements in terms of strength, ductility, and energy dissipation, as confirmed by analytical and experimental studies conducted by Shehata *et al.* (2002), Teng and Lam (2002), Xiao and Wu (2003), Berthet *et al.* (2005), Barros and Ferreira (2008), Benzaid and Mesbah (2013), Vincent and Ozbakkaloglu (2015), Shayanfar and Akbarzadeh (2018), and Suon *et al.* (2019).

Real reinforced concrete (RC) columns have always a certain percentage of steel hoops, which ensures some concrete confinement. Therefore, some researchers (Perrone *et al.* (2009), Mai *et al.* (2018) and Janwaen *et al.* (2019)) have demonstrated that the application of FRP strips between existing steel hoops can be a strengthening technique of proper compromise in terms of confinement effectiveness and cost competitiveness for this type of structural elements. However, the application of discrete FRP strips might pose less confinement efficiency compared to full confinement configuration, as confirmed by experimental studies conducted by Barros and Ferreira (2008), Zeng *et al.* (2017, 2018a and 2018b), Wang *et al.* (2018), Guo *et al.* (2018 and 2019). Barros and Ferreira (2008) experimentally investigated the confinement efficiency in the case of circular RC columns partially confined with different carbon fiber-reinforced polymer (CFRP) configurations. The test results revealed that the axial response of RC columns in terms of strength and deformability can be improved by increasing the thickness and the width of the CFRP jacket. The confinement efficiency was also verified to be noticeably dependent on the distance between CFRP strips.

To evaluate the effectiveness of a FRP confining system for axial strengthening of concrete columns, several theoretical models have been developed. These models generally can be categorized in two distinctive groups: design-oriented and analysis-oriented models. In general, the former group provides an estimation of the ultimate axial capacity, whereas the latter determines axial stress at any level of axial strain. A comprehensive review of available models in the literature can be found in Ozbakkaloglu *et al.* (2013) and Huang *et al.* (2016). In the analysis-oriented models a relationship between concrete lateral expansion (representative of dilation behavior) and axial strain is considered. Consequently, their predictive performance highly depends on the reliability of this relation. In this regard, several analytical models have been proposed to predict dilation behavior of FRP confined concrete. In case of fully confined concrete columns of circular cross section, Mirmiran and Shahawy (1997) proposed a dilation model to predict the tangential Poisson's ratio (the rate of change of lateral strain with respect to axial strain as shown in Fig. 1) versus axial strain relation, depending on the confinement stiffness parameter (known as the ratio of confinement pressure over lateral strain). Furthermore, Xiao and Wu (2003) derived a relation between secant Poisson's ratio (the ratio between lateral strain and axial strain, as shown in Fig. 1) and axial strain, which is a function of unconfined concrete compressive strength and confinement stiffness. For fully confined concrete elements of circular cross section, Teng *et al.* (2007) and Lim and Ozbakkaloglu (2014a) proposed lateral strain versus axial strain relations dependent on the level of confinement pressure. In the case of partial confinement, Zeng *et al.* (2018a) adopted Teng *et al.* (2007) dilation model by applying a reduction factor in the confinement pressure due to the vertical arching action. It should be noteworthy that the existing dilation models were formulated for fully confined concrete columns and calibrated based on the results from experimental tests with this type of specimens, therefore their applicability for partial confining system is, at least, arguable.

Regarding the partial confinement system, the concrete at the middle distance between FRP strips, hereafter designated by critical section, would experience more lateral expansion compared to the concrete at the strip regions, as confirmed by Guo *et al.* (2018 and 2019) and Zeng *et al.* (2018a). Particularly, for the case of partial confinement configuration with a large distance between FRP strips, the concrete expansion at the strip regions might not be strong enough to considerably activate FRP confining stress (Barros and Ferreira (2008) and Wang *et al.* (2018)). To the best of the authors' knowledge, the impact of non-uniform lateral expansion of concrete on the confinement efficiency has not been addressed comprehensively in the existing formulations. Accordingly, a generalized dilation model applicable for both full and partial confinement configurations, considering the effect of non-uniform expansion, is still lacking.

In this study, a new dilation model is developed by considering the confinement stiffness for both full and partial confinement configurations. This model takes into account the influence of non-uniform distribution of concrete lateral expansion on the confinement stiffness. For this purpose, relations between secant Poisson's ratio versus axial strain at critical section and at mid-plane of FRP strips are proposed. Based on the assembled database of test results, available in the literature, of fully and partially FRP confined concrete specimens, the reliability and the good predictive performance of the developed model is demonstrated.

Concept of confinement efficiency factor

During axial loading, in a partial confinement system, the vertical arching action between the strips induces concrete regions of different confinement level. Accordingly, the axial compressive stress of a FRP partially confined concrete can be assumed to be carried through two separate components corresponding to the areas where confinement is effective and ineffective. With the determination of the axial stress versus axial strain relationships of each area, the entire uniaxial stress-strain curve of FRP partially confined concrete can be calculated. On the other hand, for the sake of simplicity, a reduction factor is applied to the confinement stress (f_l) acting on the effectively confined area in order to reduce the confinement pressure actuating on the whole cross-section. This reduction factor is generally called "*confinement efficiency factor,* K_e". Accordingly, the whole cross-section can be assumed to be uniformly subjected to an effective confinement stress $f'_l = K_e \times f_l$.

In the case of steel partially confined concrete, Mander *et al.* (1988) proposed an empirical equation to calculate K_e as A_{eff} / A_g in the determination of confinement characteristics of peak axial stress; where A_{eff} is the effectively confined concrete core area at the critical section (at the middle of the clear distance between two adjacent steel hoops) and A_g is the entire concrete area. Accordingly, assuming a second order parabola function with the vertical arching angle equal to 45°, K_e can be obtained as:

$$K_e = \frac{A_{eff}}{A_g} = \left(\frac{D'}{D}\right)^2 = \left(\frac{D - \frac{s'}{2}}{D}\right)^2 = \left(1 - \frac{s'}{2D}\right)^2 \quad (1)$$

where D is the diameter of the column's cross section; D' is the diameter of the effectively confined concrete at the critical section; s' is the clear distance between two adjacent steel hoops. This approach has been adopted for the case of FRP partially confined concrete, by substituting s' in Eq. (1) with s_f (the clear distance between two adjacent FRP strips as shown in Fig. 2) (see *fib* Bulletin No. 14 (2001), CNR-DT 200 (2004), and ACI 440.2R-08 (2008)).

A closer examination of the concept of confinement efficiency factor developed by Mander *et al.* (1988) reveals that this model only empirically addresses the detrimental effect of the vertical arching action on the confinement pressure at the critical section defined at the middle distance between two consecutive confining materials. However, in partial FRP confinement configurations, the critical section, in addition of the lowest confinement pressure, experiences the maximum concrete lateral expansion, while the lowest concrete expansion occurs at the strip region due to the highest FRP confining pressure. In this regard, the distance between two consecutive FRP strips plays a key role for the confinement efficiency of FRP partial configuration. In the case of relatively large distance between FRP strips, the concrete expansion is similar to that of unconfined concrete and it might not be strong enough at the strip regions to considerably activate FRP confining stress (Barros and Ferreira (2008) and Wang *et al.* (2018)). Accordingly, in partial FRP confinement configurations, in addition to the vertical arching action, the impact of concrete lateral expansion should be taken into account on the determination of K_e.

Concrete lateral expansion

Fig. 2 illustrates a typical concrete column of circular cross section partially confined by FRP strips. The region of the RC column, composed by an influencing width of FRP strip of $w_f / 2$ and a clear distance of s_f, is assumed representative of a partial confinement region for the determination of axial and dilation behavior of the confined column during axial loading. As shown in Fig. 3a, in a partial confinement configuration, the critical section, at the middle distance between FRP strips, experiences the maximum concrete lateral expansion, $\varepsilon_{l,j}$ (the "*j*" in the subscript aims to represent the halfway between two adjacent FRP strips). It is noteworthy that the experimental results evidenced that at the stage close to failure, the increase of the concrete lateral strain occurs more rapidly at the mid-height of the unconfined zone as confirmed by Guo *et al.* (2019). Due to the lack of sufficient experimental results in the literature to reliably evidence the pattern of concrete lateral strain variation between two adjacent strips, in the present study, this pattern was inspired by the pattern of vertical arching action but in the opposite direction (expansion direction), with the strain gradient equal to zero at the critical section. Furthermore, based on the experimental observation reported by Zeng *et al.* 2018b, a uniform concrete lateral distribution was assumed for the strip zone, evenly subjected to FRP confining stress. As can be seen in Fig. 3a, for a certain $\varepsilon_{l,j}$, concrete at the mid-plane of the FRP strips experiences lower dilatancy ($\varepsilon_{l,i}$) due to the fact that this area is directly subjected to FRP confinement pressure (the "*i*" in the subscript aims to represent the mid-plain of the FRP strips). Here, k_ε is defined as the ratio between concrete lateral strain at the strip mid-plane and at the critical section ($k_\varepsilon = \varepsilon_{l,i} / \varepsilon_{l,j}$). Accordingly, assuming that lateral (radial) and hoop (circumferential) strains are identical, FRP tensile strain $\varepsilon_{h,P}$ at strip region would be equal to $\varepsilon_{h,P} = \varepsilon_{l,i} = k_\varepsilon \varepsilon_{l,j}$ (the "*P*" in the subscript aims to represent a strain concept in a partial wrapping confinement configuration). In the case of full confinement presented in Fig. 3b, existing models (*fib* Bulletin No. 14 (2001), CNR-DT 200 (2004), ACI 440.2R-08 (2008)) assume that the column subjected to axial loading would experience a uniform distribution of lateral expansion $\varepsilon_{l,i} = \varepsilon_{l,j}$ (this simplification is quite acceptable up to the compressive strength of unconfined concrete as evidenced by Guo *et al.* (2018)). Hence, considering FRP hoop strain $\varepsilon_{h,F} = \varepsilon_{l,j}$ (the "*F*" in the subscript aims to represent a strain concept in a full wrapping confinement configuration), FRP confining stress f_f is equal to $E_f \varepsilon_{l,j}$. Therefore, at a certain level of $\varepsilon_{l,j}$, the ratio of FRP confining stress in the cases of partial and full configurations, named as f'_f and f_f, respectively, is:

$$\frac{f'_f}{f_f} = \frac{E_f \varepsilon_{h,P}}{E_f \varepsilon_{h,F}} = \frac{\varepsilon_{l,i}}{\varepsilon_{l,j}} = k_\varepsilon \tag{2}$$

As a result, at a certain level of axial stress f_c (corresponding to ε_c), full and partial confinement configurations generate FRP confining stress equal to f_f and $k_\varepsilon f_f$, respectively. In fact, the reduction factor k_ε addresses the influence of non-uniform distribution of concrete lateral expansion in the determination of FRP confining stress, and it can be assumed to be a function of the distance between FRP strips, s_f. The maximum value of k_ε ($k_{\varepsilon,max}$) is equal to 1 in the case of full confinement with $s_f = 0$, while the minimum value of k_ε ($k_{\varepsilon,\min}$) might occur in the case of partially confined concrete with a relatively large s_f, resulting in extensive damage around the critical section (concrete transverse expansibility), and marginal concrete dilation at the two end confined regions. In other words, in the case of relatively large s_f, the critical section can be assumed to behave like unconfined concrete with abrupt increase in expansibility when concrete experiences ultimate axial strain ε_{cu}, leading to a large concrete volumetric expansion, while concrete at the mid-plane of the FRP strips remains in the maximum confinement stage. Based on the dilation responses of a series of unconfined concrete specimens tested by Osorio *et al.* (2013), $\varepsilon_{l,j}$ corresponding to $\varepsilon_{cu} = 0.004$ was assumed to approximately equal to 0.01, inducing an ultimate secant Poisson's ratio $v_{s,u}^{unc} = \varepsilon_{l,j} / \varepsilon_{cu} = 2.5$. Assuming the elastic behavior with initial Poisson's ratio of $v_i = 0.2$ for the concrete located at the mid-plane of FRP strips, $\varepsilon_{l,i}$ would be equal to 0.0008 ($\varepsilon_{l,i} = v_i \varepsilon_{cu}$). Accordingly, for confined concrete with a relatively large s_f, the ratio of concrete expansion at the critical section (assumed as unconfined concrete) and at the mid-plane of FRP strip, representative of $k_\varepsilon = k_{\varepsilon,min}$, can be calculated as $\varepsilon_{l,i} / \varepsilon_{l,j} = 0.08$, whereas in the case of full confinement with $s_f = 0$, k_ε is equal to 1.

In the present study, to formulate the relation between k_ε and s_f, a set of the experimental dilation results reported by Barros and Ferreira (2008), Wang *et al.* (2018), Zeng *et al.* (2018a and 2018b) was used. For partially FRP confined concrete specimens with $s_f > 0.75D$, Wang *et al.* (2018) demonstrated that the FRP confinement effectiveness, even with thick FRP jacket, would be minimal in compliance with the experimental observations reported by Barros and Ferreira (2008). Likewise, according to the failure mode of the test results reported by Zeng *et al.* (2018a and 2018b), for specimens with a relatively large s_f, the concrete between two adjacent FRP strips is highly expected to experience concrete crushing failure, instead of simultaneous FRP rupture/concrete crushing failures. Details of the reported dilation results of the test specimens with a relatively large s_f / D and marginal confinement efficiency (determined as f_{cc}^{exp} / f_{c0}) can be found in Table 1, where f_{cc}^{exp} is the experimental peak axial stress of confined concrete, and f_{c0} is the peak axial stress of unconfined concrete. In this table, $v'_{s,u}{}^{exp}$ represents the ultimate secant Poisson's ratio at the mid-plane of FRP strips (obtained experimentally as the ultimate ratio of FRP tensile strain $\varepsilon_{h,P}$ recorded by strain gauge and corresponding axial strain ε_c in the column). In the present study, with a slightly conservative assumption, the ultimate secant Poisson's ratio of the test specimens at the critical section, $v_{s,u}^{exp}$, was taken into account equal to 2.5, similar to that of unconfined concrete. Then, k_ε^{exp} can be calculated as $v'_{s,u}{}^{exp} / 2.5$.

Fig. 4 demonstrates the proposed relation between k_ε and s_f / D, determined based on the experimental dilation results. As can be seen, k_ε can be reasonably assumed to decrease linearly from 1 at $s_f = 0$ (full confinement) to 0.08 at $s_f = D$, as:

$$k_{\varepsilon} = 1 - 0.92 \frac{s_f}{D} \qquad \text{for } \frac{s_f}{D} \leq 1 \tag{3a}$$

$$k_{\varepsilon} = 0.08 \qquad \text{for } \frac{s_f}{D} \geq 1 \tag{3b}$$

As shown in Fig. 4, for $s_f / D \geq 1$, the dilation response of FRP partially confined concrete tends to be similar to unconfined concrete, since FRP confining stress $f'_f = k_{\varepsilon} f_f$ is not capable of limiting transversal concrete deformation. Furthermore, the proposed relationship between k_{ε} and s_f seems to provide good agreement with the test data.

Vertical arching action

Fig. 5 illustrates the uniform and non-uniform distribution of confinement pressure in full and partial confinement arrangements, respectively. For partial arrangements, the maximum and minimum influence of the confinement pressure on the dilation behavior of concrete would occur at mid-plane of FRP strips and at critical section, respectively. Here, $f_{l,i}$ is the confinement pressure generated by FRP confining stress f'_f at the strip region. In the present study, due to the nonlinear distribution of confinement pressure in a partial arrangement, a reduction factor k_v is proposed to simulate the confinement distribution as uniform with a constant confinement pressure called "*effective confinement pressure*" applied on the whole concrete:

$$f'_l = k_v \times f_{l,i} \tag{4}$$

Contrarily, in the case of full confinement, there is a constant distribution of confinement pressure, equal to $f_{l,i} = f_{l,j} = f_l$ developed by FRP confining stress f_f (Fig. 5b). Here, $f_{l,j}$ defines the confinement pressure at the middle height of the column, equal to that at the strip regions. Since confinement pressure is a function of the confining stress (Mander *et al.* 1988), the ratio of confinement pressure in partial ($f_{l,i}$) and full ($f_{l,j} = f_l$) confinement arrangements can be as:

$$\frac{f_{l,i}}{f_l} = \frac{f'_f}{f_f} \rightarrow f_{l,i} = \frac{f'_f}{f_f} \times f_l \tag{5}$$

Replacing Eq. (2) into Eq. (5) gives:

$$f_{l,i} = k_\varepsilon \times f_l \tag{6}$$

Therefore, putting Eq. (6) into Eq. (4), the effective confinement pressure, f'_l, would be:

$$f'_l = k_v k_\varepsilon f_l = K_e f_l \tag{7}$$

in which

$$K_e = k_v k_\varepsilon \tag{8}$$

where K_e defines the efficiency confinement factor as a function of k_ε and k_v, as shown in Fig. 5. Hence, the determination of the reduction factor k_v in Eq. (8) is necessary, as an input parameter for partial confinement arrangements. In this regard, for the case of partial confinement arrangement, considering nonlinear and constant distributions of confinement pressure (Fig. 5a) and, the equilibrium of confinement forces results in:

$$k_v f_{l,i}\left(s_f + w_f\right)D = 2 f_{l,i}\frac{w_f}{2}D + 2\int_0^{s_f/2} f_z d_z dx \rightarrow k_v = \frac{f_{l,i} w_f D + 2\int_0^{s_f/2} f_z d_z dx}{f_{l,i}\left(s_f + w_f\right)D} \tag{9}$$

where w_f is the FRP width; f_z and d_z are the functions of FRP lateral pressure and the diameter of effective confinement area, respectively, as shown in Fig. 5a. It should be noted that the diameter of the effective confinement area decreases from D to D' due to arching action, as illustrated in

Fig. 5a. In the present study, according to the geometric constraints provided by Eqs. (12) and (13), two separate second order parabola functions for f_z and d_z were assumed in compliance with the vertical arching angle equal to 45° (Mander *et al.* 1988) as:

$$f_z = a_1 x^2 + a_2 x + a_3 \tag{10}$$

$$d_z = b_1 x^2 + b_2 x + b_3 \tag{11}$$

in which

$$f_z\left(x = 0\right) = f_{l,i} \tag{12a}$$

$$f_z\left(x = \frac{s_f}{2}\right) = f_{l,j} \tag{12b}$$

$$\frac{df_z}{dx}\left(x = \frac{s_f}{2}\right) = 0 \tag{12c}$$

and

$$d_z\left(x = 0\right) = D \tag{13a}$$

$$d_z\left(x = \frac{s_f}{2}\right) = D' = D - \frac{s_f}{2} \tag{13b}$$

$$\frac{dd_z}{dx}\left(x = \frac{s_f}{2}\right) = 0 \tag{13c}$$

To derive the minimum confinement pressure at the critical section, $f_{l,j}$, as demonstrated in Fig. 5, it was assumed that $f_{l,j} = f_{l,i}$ and $f_{l,j} = 0$ in the cases of confined concrete with $s_f = 0$ and $s_f \geq 2D$, respectively. It should be noted that when $s_f / D = 2$, due to the vertical arching action (assumed as a second order parabola equation with the vertical arching angle equal to 45°), the diameter of effective confined area at the critical section is zero. Consequently, confinement pressure could not restrain concrete expansion at this section. Accordingly, the relationship of $f_{l,j}$ and s_f as a second order parabola equation is:

$$f_{l,j} = \left(1 - \frac{s_f}{D} + 0.25\left(\frac{s_f}{D}\right)^2\right) f_{l,i} \qquad \text{for } \frac{s_f}{D} < 2 \tag{14a}$$

$$f_{l,j} = 0 \qquad \text{for } \frac{s_f}{D} \geq 2 \tag{14b}$$

According to the geometric constraints (Eqs. (12) and (13)), f_z and d_z equations are:

$$f_z = \left[\left(\frac{4}{Ds_f} - \frac{1}{D^2}\right)x^2 - \left(\frac{4}{Ds_f} - \frac{1}{D^2}\right)s_f x + 1\right] f_{l,i} \tag{15}$$

$$d_z = \left[\left(\frac{2}{Ds_f}\right)x^2 - \left(\frac{2}{D}\right)x + 1\right] D \tag{16}$$

Introducing Eqs. (15) and (16) into Eq. (9), and then solving the integration leads to:

$$k_v = \frac{f_{l,i} w_f D + f_{l,i} D s_f \left(1 - \frac{s_f}{D} + \frac{13 s_f^{\,2}}{30 D^2} - \frac{s_f^{\,3}}{15 D^3}\right)}{f_{l,i} \times \left(s_f + w_f\right) D} \tag{17}$$

Rearranging Eq. (17) gives:

$$k_v = \frac{w_f + s_f \left(1 - \frac{s_f}{D} + \frac{13 s_f^{\,2}}{30 D^2} - \frac{s_f^{\,3}}{15 D^3}\right)}{s_f + w_f} \leq 1 \tag{18}$$

As a result, Eq. (8) can be rewritten as:

$$K_e = k_v k_\varepsilon = \frac{w_f + s_f\left(1 - \frac{s_f}{D} + \frac{13{s_f}^2}{30D^2} - \frac{{s_f}^3}{15D^3}\right)}{s_f + w_f}\left(1 - 0.92\frac{s_f}{D}\right) \qquad \text{for } \frac{s_f}{D} < 1 \tag{19a}$$

$$K_e = k_v k_\varepsilon = 0.08\frac{w_f + s_f\left(1 - \frac{s_f}{D} + \frac{13{s_f}^2}{30D^2} - \frac{{s_f}^3}{15D^3}\right)}{s_f + w_f} \geq 0 \qquad \text{for } \frac{s_f}{D} \geq 1 \tag{19b}$$

Based on the preliminary sensitivity analysis of the parameters in Eq. (19), for further simplification, a simplified equation was developed as a linear function of s_f / D and w_f / D as follows:

$$K_e = 0.97 + 0.12\frac{w_f}{D} - 1.25\frac{s_f}{D} \leq 1 \qquad \text{for } s_f / D < 0.5 \tag{20a}$$

$$K_e = 0.75 + 0.12\frac{w_f}{D} - 0.79\frac{s_f}{D} \geq 0.04 \qquad \text{for } 0.5 \leq s_f / D \leq 1 \tag{20b}$$

$$K_e = 0.04 - 0.02\left(\frac{s_f}{D} - 1\right) \geq 0 \qquad \text{for } s_f / D \geq 1 \tag*{(20b)}$$

Fig. 6 demonstrates analytically the variation of the proposed K_e with s_f / D. As can be seen in Fig. 6a, the good agreement between the results obtained from Eq. (19) and the simplified Eq. (20) confirms the reliability of the simplification. In addition, it highlights the relative higher influence of k_ε for the final value of K_e compared to k_v. In Fig. 6b, the comparison of K_e obtained from Eq. (1) developed by Mander *et al.* (1988) with Eq. (20) shows that the proposed model predicts K_e values lower than those determined by Eq. (1). It can be attributed to the consideration of the detrimental effect of k_ε, in addition to the vertical arching action, in the determination of the proposed K_e. Furthermore, the results confirm that, for the same s_f / D, the increase of w_f / D does not seem to have significant alteration in K_e.

Effective lateral confining pressure

In Fig. 7, the confining action in fully and partially FRP confined concrete columns with circular cross section is schematically represented. As shown in Fig. 7a, for a certain axial stress f_c installed in a full FRP confinement configuration, the corresponding FRP tensile stress, f_f, induces a uniform lateral confinement pressure, f_l, acting on the entire concrete area in contact with the FRP. To derive f_l generated by f_f for a full FRP confinement configuration, the equilibrium of forces in the concrete column at the section A-A shown in Fig. 7a must be assured:

$$f_l \left(s_f + w_f \right) D = 4 f_f n_f t_f \frac{w_f}{2} \tag{21}$$

where n_f and t_f are the number of FRP layers and thickness of each layer, respectively. Consequently, rearranging Eq. (21) gives:

$$f_l = \frac{2 n_f t_f w_f}{\left(s_f + w_f \right) D} f_f = \frac{2 n_f t_f w_f}{\left(s_f + w_f \right) D} E_f \varepsilon_{h,F} = \frac{2 n_f t_f w_f}{\left(s_f + w_f \right) D} E_f \varepsilon_{l,j} \tag{22}$$

where E_f is the FRP modulus elasticity. Now if p_f defines the ratio of the volume of fibers, V_{FRP}, to the volume of concrete, V_{con}, then:

$$\rho_f = \frac{V_{FRP}}{V_{con}} = \frac{2 \pi D n_f t_f \dfrac{w_f}{2}}{\dfrac{\pi D^2}{4} \left(w_f + s_f \right)} = \frac{4 n_f t_f w_f}{D \left(w_f + s_f \right)} \tag{23}$$

Substituting Eq. (23) into Eq. (22), and then rearranging, yields:

$$f_l = \frac{1}{2}\rho_f E_f \varepsilon_{l,j} \tag{24}$$

Therefore, in the case of partial confining system, introducing Eq. (24) into Eq. (7) gives:

$$f'_l = \frac{1}{2}K_e \rho_f E_f \varepsilon_{l,j} \tag{25}$$

On the other hand, considering the secant Poisson's ratio, v_s, at the critical section as $\varepsilon_{l,j} / \varepsilon_c$ (Fig. 7b), Eq. (25) results in:

$$f'_l = \frac{1}{2}K_e \rho_f E_f v_s \varepsilon_c \tag{26}$$

Accordingly, if ε_c is first specified, then by just addressing the corresponding v_s, effective confinement pressure f'_l can be calculated by Eq. (26). Once its relation with ε_c is available, axial stress, f_c, versus ε_c relationship for fully and partially FRP confined concrete can easily be calculated following the active confinement approach, as recommended by existing analysis-oriented models (e.g. Lim and Ozbakkaloglu (2014b)).

Dilation response

In this section, the determination of a relation between v_s (corresponding to $\varepsilon_{l,j}$) and the applied axial strain level in the concrete column, ε_c, is performed. For a preliminary evaluation of dilation behavior of fully and partially FRP wrapped concrete, the experimental results reported by Zeng *et al.* (2018a) are analyzed, as shown in Fig. 8. For this purpose, the test specimens wrapped by two FRP layers with different s_f / D are selected. Peak axial compressive stress of unconfined concrete, f_{c0}, was reported as 23.4 MPa. Here, ρ_K defines the confinement stiffness index, as recommended by Teng *et al.* (2009) for fully FRP confined circular concrete columns. However, in the present study, this non-dimensional parameter index is extended for the case of partial confinement arrangements by adopting the concept of confinement efficiency factor, as:

$$\rho_K = \frac{f'_l/\varepsilon_{l,j}}{f_{c0}/\varepsilon_{c0}} = \frac{1}{2}K_e \frac{\rho_f E_f}{f_{c0}/\varepsilon_{c0}} \tag{27}$$

in which

$$\varepsilon_{c0} = 0.0015 + \frac{f_{c0}}{70000} \qquad \text{(Karthik and Mander (2011))} \tag{28}$$

where f_{c0} is in MPa. Moreover, the volumetric strain, ε_V, is expressed as:

$$\varepsilon_V = \varepsilon_c + \varepsilon_r + \varepsilon_h = \varepsilon_c + 2\varepsilon_h = \varepsilon_c - 2\varepsilon_{l,j} \tag{29}$$

where ε_r and ε_h are the lateral (radial) and hoop circumferential strains, respectively. Tensile strain (ε_h) and volumetric expansion are assumed to be negative, while compressive strain (ε_c) and volumetric compaction are considered positive. It should be noted that for comparison, typical axial and dilation responses of unconfined concrete, determined based on Mander *et al.* (1988) and Osorio *et al.* (2013), are also presented in Fig. 8. Furthermore, $\varepsilon_V < 0$ and $\varepsilon_V > 0$ mean a concrete volumetric expansion and compaction, respectively, during axial compressive loading, and $\varepsilon_V = 0$ corresponds to the secant Poisson's ratio (v_s) equal to 0.5, where concrete volume is not changing. As shown in Fig. 8a, up to roughly f_{c0} and prior the transition zone, the confined concrete tends to behave similar to the unconfined concrete. In transition stage, concrete experiences a significant stiffness degradation along with an increase in the rate of its lateral expansion, leading to the activation of FRP confining pressure. In the case of unconfined concrete, beyond the transition zone, the volumetric change evolution is suddenly reversed due to the degeneration of micro- into meso- and macro-cracks in concrete, leading to a large volumetric expansion (Figs. 8b and c). On the other hand, for FRP confined concrete, after the transition zone, the activated lateral confinement pressure tends to restrain the concrete lateral expansion. In other words, lateral pressure applied by the FRP jacket acts in a way to counteract the tendency of concrete for stiffness degradation (Fig. 8b to d). Accordingly, considering the influence of confinement pressure in counteracting the concrete expansion tendency, the volumetric change can be regarded as a function of the confinement stiffness, ρ_K. For the high level of this stiffness factor, due to FRP jacket capability to curtail the concrete expansion, its axial strength and deformability can increase significantly. In this way, FRP confined concrete might fail with experiencing a large volume compaction, as shown in Fig. 8c. However, for low level of ρ_K, confined and unconfined concrete have similar dilation response, due to the insufficient confinement pressure in the former one.

A closer look of the dilation behavior of the test specimens with $s_f / D = 0.25$ and 0.44 reveals that the effect of s_f on the confinement stiffness was significant enough to alter the tendency of the volumetric response. In fact, the v_s versus ε_c curve of these specimens in Fig. 8d demonstrates that for $s_f / D = 0.25$, the maximum secant Poisson's ratio ($v_{s,max}$) has occurred at $\varepsilon_{c,m} = 0.0067$, above which the FRP lateral pressure has restrained concrete dilation, resulting in a remarkable decrease in v_s. However, for $s_f / D = 0.44$, $v_{s,max}$ occurred at the axial strain of $\varepsilon_{c,m} = 0.0136$, corresponding to the ultimate concrete axial strain. Accordingly, confinement pressure was not capable of changing the concrete expansion evolution during axial loading. In this case, despite of a slight decrease in v_s corresponding to $\varepsilon_c = 0.009$, the lateral pressure provided by FRP was not enough to continue restraining the concrete dilation response for $\varepsilon_c > 0.011$.

Proposed relation of v_s versus ε_c

In this section, the determination of v_s versus ε_c relation for fully and partially FRP confined concrete based on experimental results is performed. For this purpose, a large database consisting of 289 test specimens was collected, whose details can be found in Table 2. This data corresponds to the experimental studies reporting the column dilation behavior available in the literature. Among the tested specimens, 153 specimens were fully FRP confined concrete and 136 specimens were confined by partially wrapping concrete with FRP strips. The criteria considered to select the experimental data available in the literature are as follows: (i) Test specimens subjected to axial compressive loading; (ii) Circular concrete columns without steel hoops/ties; (iii) Test specimens fully/partially confined by FRP; (iii) Availability of experimental FRP hoop strain versus axial strain relation (iv) Fibers oriented 90° with respect to the column longitudinal axis. In the test database, f_{c0} is in the range of 15.8–171 MPa with mean and CoV of 40.1 MPa and 0.59, respectively. Types of FRP materials consist of: carbon (CFRP), basalt (BFRP), glass (GFRP) and aramid (AFRP) with E_f ranging 13.6–276 GPa with mean and CoV of 184.3 GPa and 0.4, respectively; $n_f \times t_f$ (total thickness of FRP strips) ranging 0.11-3.78 mm with mean and CoV of 0.56 mm and 0.79, respectively; ρ_K is in the range of 0.002–0.262 with mean and CoV of 0.037 and 0.85, respectively. The experimental $v_{s,max}$ is in the range of 0.25–5.31 with mean and CoV of 1.1 and 0.65, respectively. To extract the value of the maximum secant Poisson's ratio, $v_{s,max}$, corresponding to the concrete critical section located in the middle of two adjacent FRP strips from the partially confined tests, experimental $\varepsilon_{h,P}$ versus ε_c relations were firstly converted to $\varepsilon_{l,j}$ versus ε_c relations using Eq. (3). By considering that $v_s = \varepsilon_{l,j} / \varepsilon_c$, the previous relation is transformed into a v_s versus ε_c relation, from which $v_{s,max}$ is determined. As shown in Fig. 8d, the parameter $v_{s,max}$ plays a key role in dilation response of FRP confined concrete.

For further examination, Fig. 9 shows the influence of ρ_K on the variation of the experimental $v_{s,max}$ in full and partial concrete confinement arrangements. As can be seen, in the case of fully confined concrete, $v_{s,max}$ decreases considerably with the increase of ρ_K, which means that as higher is ρ_K as smaller is the concrete dilation. Fig. 9a evidences that for partially confined concrete, the relation between $v_{s,max}$ and ρ_K determined by the proposed approach exhibits almost the same trend with that of full confinement. On the other hand, the relation between $v^*_{s,max}$ and ρ^*_K is shown in Fig. 9b, where ρ^*_K denotes the confinement stiffness index derived from the original concept of the confinement efficiency factor, developed by Mander *et al.* (1988) (it can be calculated by Eq. (27) using K_e in Eq. (1)) and $v^*_{s,max}$ is the maximum secant Poisson's ratio, determined based on $k_\varepsilon = 1$ because the impact of concrete expansion distribution was ignored by Mander *et al.* (1988). As can be seen in Fig. 9b, at a certain value of ρ^*_K, $v^*_{s,max}$ of the partially confined specimens seems to be lower than that of full confinement counterpart, especially for low level of ρ^*_K. It presents better dilation behavior for partial systems, compared to fully confined concrete with same ρ^*_K. This can be attributed to the fact that in the Mander *et al.* (1988) approach, the non-uniform distribution of concrete lateral expansion is not considered in the determination of K_e.

Based on the best-fit of the dilation results in the test database, the following equation was derived for determining $v_{s,max}$ from ρ_K and f_{c0}:

$$v_{s,\max} = \frac{0.155}{\left(1.23 - 0.003 f_{c0}\right)\sqrt{\rho_K}} \qquad (f_{c0} \text{ in MPa}) \tag{30}$$

To assess the reliability of this relation, Fig. 10 compares the results obtained from Eq. (30) with those extracted from the experimental tests. The values of the mean, coefficient of variation, CoV, and mean absolute percentage error, MAPE, reported in Fig. 10, evidence the good predictive performance of the proposed equation to estimate the value of $v_{s,max}$ in fully and partially FRP confined concrete.

Determination of $v_s / v_{s,max}$ versus ε_c relation

In this section, the relation between $v_s / v_{s,max}$ and ε_c corresponding to dilation behavior at the critical section between strips is derived. Based on dilation responses extracted from the experimental results, the diagram represented in Fig. 11 is proposed to predict the dilation behavior of fully and partially FRP confined concrete columns of circular cross section. In this figure, $\varepsilon_{c,m}$ is the axial strain corresponding to $v_{s,max}$; c_1, c_2, c_3 and c_4 are the non-dimensional empirical coefficients depending on the axial strain level and ρ_K. According to the best curve fit of the experimental results by using a back analysis, these parameters were determined as:

$$\varepsilon_{c,m} = 0.0085 - 0.05\rho_K \tag{31}$$

and

$$c_1 = 0.75 + 3.85\rho_K < 1.00 \tag{32a}$$

$$c_2 = 0.85 + 1.54\rho_K < 0.95 \tag{32b}$$

$$c_3 = 0.65 + 3.08\rho_K < 0.85 \tag{32c}$$

$$0.5 < c_4 = 0.20 + 9.23\rho_K < 0.80 \tag{32d}$$

$$v_{s,0} = 8\times10^{-6} f_{c0}{}^2 + 2\times10^{-4} f_{c0} + 0.138 \quad (f_{c0} \text{ in MPa}) \tag{33}$$

where $v_{s,0}$ is the initial Poisson's ratio of concrete, determined as recommended by Candappa *et al.* (2001). As shown in Fig. 11, the expansion of confined concrete is equal to unconfined concrete up to $\varepsilon_c = \varepsilon_{c0}$ (point A) with $v_s = v_{s,0}$. After which, the development of concrete cracking induces an increase in v_s. Subsequently, concrete secant Poisson's ratio tends to increase from $v_{s,0}$ to $c_1 \times v_{s,max}$, corresponding to $\varepsilon_c = 2\varepsilon_{c0}$ (Mander *et al.* 1988). In this phase, FRP confinement pressure is activated by restraining concrete tendency to dilate. The trend afterward $v_{s,max}$ has been reached, at $\varepsilon_c = \varepsilon_{c,m}$ (point C), is followed by a drop in the rate of concrete lateral expansion until ultimate conditions.

To examine the reliability of the proposed relation, its prediction, for different levels of ρ_K, is compared with the experimental results in Fig. 12. It should be noted that the analytical relation in each figure is calculated by adopting the average value of the corresponding interval of ρ_K values. As can be seen in the figure, there is a good agreement between the experimental test and analytical results, confirming the reliability of the proposed design-based formulation represented in Fig. 11.

It would be noteworthy that concrete lateral expansion can be regarded as a function of the development of concrete cracking, and subsequently, of the axial strain ε_c. According to the experimental observations from Guo *et al.* (2018 and 2019), for $\varepsilon_c \le \varepsilon_{co}$ (where ε_{co} is the axial strain corresponding to peak stress of unconfined concrete f_{c0}), concrete lateral strain at the mid-plane of FRP strips and at the critical section would be virtually identical ($k_\varepsilon = 1$) due to marginal cracking. However, the ratio between concrete expansion in these regions, k_ε, decreases when $\varepsilon_c \ge 2\varepsilon_{co}$ due to the development of major concrete cracking Guo *et al.* (2018 and 2019)). Considering that $\overline{k_\varepsilon}$ defines the ratio of concrete expansion at the mid-plane of FRP strips and at the critical section, by assuming it linearly varies in the $\varepsilon_{c0} \le \varepsilon_c \le 2\varepsilon_{c0}$ interval, it can be calculated as:

$$\overline{k_\varepsilon} = 1 - (1 - k_\varepsilon)\left(\frac{\varepsilon_c}{\varepsilon_{c0}} - 1\right) \tag{34}$$

On the other hand, considering that v_s defines the dilation response at the critical section, the dilation characteristics at the mid-plane of strips (v'_s) can be determined as:

$$v'_s = v_{s,0} \qquad \text{for } \varepsilon_c \le \varepsilon_{c0} \tag{35a}$$

$$v_{s,0} \le v'_s = \overline{k_\varepsilon} v_s \le k_\varepsilon c_1 v_{s,\max} \qquad \text{for } \varepsilon_{c0} \le \varepsilon_c \le 2\varepsilon_{c0} \tag{35b}$$

$$v'_s = k_\varepsilon v_s \qquad \text{for } \varepsilon_c \ge 2\varepsilon_{c0} \tag{35c}$$

The upper bound in Eq. (35b), demonstrating secant Poisson ratio v'_s when $\varepsilon_c = 2\varepsilon_{c0}$, was taken into account due to fact that concrete lateral strain, either at the critical section or the mid-plane of strips, increasingly enhances during axial compressive loading.

A parametric analysis was performed to highlight the influence of the key parameter, s_f / D, on the dilation response of FRP partially confined concrete elements. For this purpose, a circular cross section concrete element with diameter of 150 mm and 300 mm height is assumed. The compressive strength of concrete is considered 23.4 MPa. The values of n_f, t_f, E_f and w_f are taken equal to 2, 0.167 mm, 249.1 GPa and 30 mm, respectively. Fig. 13 demonstrates the variations of $\varepsilon_{l,j}$ and $\varepsilon_{l,i}$ with ε_c for five s_f / D arrangements. As expectably, Fig. 13a shows that at a certain ε_c, the $\varepsilon_{l,j}$ increases remarkably with s_f / D. Likewise, at a certain $\varepsilon_{l,j}$, the corresponding axial strain would substantially decrease when s_f / D increases, especially for high level of ε_c. However, as shown in Fig. 13b, $\varepsilon_{l,i}$ increases significantly with the increase of s_f / D from 0 to 0.5, but for $s_f / D > 0.5$, $\varepsilon_{l,i}$ experiences a noticeable decrease due to the relatively high concrete dilation gradient in the critical region (center part between FRP strips) that leads to a strain release in the FRP confined regions. Fig. 13c compares $v_{s,max}$ and $v'_{s,max}$ (maximum secant Poisson's ratio at the critical and mid-plane of strips, respectively) at the various levels of s_f / D. It evidences that $v_{s,max}$ exponentially rises when s_f / D increases, since according to Eq. (30) ρ_K decreases with the increase of s_f / D, which confirms the results presented in Fig. 13a. In case of $v'_{s,max}$, it increases with s_f / D up to a certain level, above which it starts decreasing, by confirming the results presented in Fig. 13b. This tendency can be attributed to the effect of s_f / D on k_ε, as represented by Eq. (3) and Fig. 4, as a key parameter to determine dilation behavior at the strip region (Eq. (35)). Accordingly, increasing s_f / D, in one hand, can induce an increase in $v_{s,max}$, and on the other hand, a reduction in k_ε. Decreasing in $v'_{s,max}$ for $s_f / D > 0.75$ shows that concrete lateral expansion at the mid-plane of FRP strip is becoming marginal, leading to a significant increase in the difference between $v_{s,max}$ and $v'_{s,max}$, as highlighted by considering the relation between Δv_s and s_f / D in Fig. 13c. Ultimately, since FRP tensile strain $\varepsilon_{h,P}$ is a function of $v'_{s,max}$ and $\varepsilon_{l,i}$, concrete expansion at the strip region is highly expected do not be considerable enough to enhance $\varepsilon_{l,i}$ and subsequently $\varepsilon_{h,P}$ in partial confinement arrangement with large s_f / D. In other word, concrete expansion at this region is not capable of impressively activating FRP confining pressure.

Ultimate condition

FRP confined concrete with full and partial confinement can present the following possible failure modes: i) FRP rupture; ii) a combination of FRP rupture and concrete crushing as function of the distance between strips; iii) concrete crushing. Thus, in addition to FRP rupture, the possibility of concrete crushing should be also controlled in the determination of ultimate condition:

$$\varepsilon_{cu} = \min\left(\varepsilon_{cu,r}, \varepsilon_{cu,c}\right) \tag{36}$$

where $\varepsilon_{cu,r}$ and $\varepsilon_{cu,c}$ are the ultimate axial strain corresponding to FRP rupture and concrete crushing, respectively.

To calculate $\varepsilon_{cu,r}$, based on Eq. (3), the ultimate secant Poisson's ratio $v_{s,u}$ at the critical section corresponding to FRP rupture can be determined as

$$v_{s,u} = \frac{\varepsilon_{l,j,u}}{\varepsilon_{cu,r}} \tag{37}$$

Considering $\varepsilon_{l,i} = k_\varepsilon \times \varepsilon_{l,j}$, Eq. (37) can be written as

$$v_{s,u} = \frac{\varepsilon_{l,i,u} / k_\varepsilon}{\varepsilon_{cu,r}} = \frac{\varepsilon_{h,rup}}{k_\varepsilon \varepsilon_{cu,r}} \tag{38}$$

where $\varepsilon_{h,rup}$ is FRP hoop rupture strain. Therefore, rearranging Eq. (38) gives

$$\varepsilon_{cu,r} = \frac{\varepsilon_{h,rup}}{k_{\varepsilon} v_{s,u}} \tag{39}$$

FRP hoop rupture strain, $\varepsilon_{h,rup}$, in FRP confined concrete columns under axial loading tends to be smaller than FRP ultimate tensile strain, ε_{fu} (from flat coupon tests). In general, to estimate the value of $\varepsilon_{h,rup}$, the existing formulations use a strain-reduction factor (Lam and Teng (2003), ACI 440.2R-08 (2008), Lim and Ozbakkaloglu (2014b). Lam and Teng [38] came up with an average strain-reduction factor of 0.586 ($\varepsilon_{h,rup} = 0.586\varepsilon_{fu}$), which was adopted by ACI 440.2R-08 (2008). Based on a test database of FRP fully confined circular concrete, Lim and Ozbakkaloglu (2014b) proposed a strain-reduction factor as a function of f_{co} and E_f. In this study, according to the test data of FRP fully confined concrete (Table 2), ACI 440.2R-08 (2008) was modified using regression analysis as:

$$\frac{\varepsilon_{h,rup}}{\varepsilon_{fu}} = 0.586\beta \tag{40}$$

in which

$$\beta = \frac{1}{0.82 + 0.23\varepsilon_{fu} f_{c0}} \tag{41}$$

As shown in Table 3, the proposed equation results in a slight improvement of ACI 440.2R-08 (2008) in the prediction of the test results of $\varepsilon_{h,rup}$, compared to other models. It should be noted that $\varepsilon_{cu,r}$ in Eq. (39) is a function of $v_{s,u}$ as an input parameter, which can be obtained from the proposed relation between v_s and ε_c (Fig. 11). Accordingly, at a certain level of ε_c, the corresponding v_s can be introduced in Eq. (39) based on the assumption of $v_{s,u} = v_s$ and then, $\varepsilon_{cu,r}$ can be calculated. If $\varepsilon_{cu,r} = \varepsilon_c$, the adopted assumption can be verified and ultimate axial strain corresponding to FRP rupture failure mode is determined.

On the other hand, to calculate $\varepsilon_{cu,c}$, according to Tamuzs *et al*. (2006), the slope of lateral-to-axial strain relation, between two points of the axial strains of $2\varepsilon_{c0}$ and $\varepsilon_{cu,c}$ was defined as the effective tangential Poisson's ratio of $v_{t,eff}$ as (Fig. 14a):

$$v_{t,eff} = \frac{\varepsilon_{l,j,u} - \varepsilon_{l1}}{\varepsilon_{cu,c} - 2\varepsilon_{c0}} \tag{42}$$

where ε_{l1} and $\varepsilon_{l,j,u}$ are the lateral strains at the critical section corresponding to $2\varepsilon_{c0}$ and $\varepsilon_{cu,c}$, respectively, when concrete crushing occurs. Rearranging Eq. (42) gives:

$$\varepsilon_{cu,c} = 2\varepsilon_{c0} + \frac{\varepsilon_{l,j,u} - \varepsilon_{l1}}{v_{t,eff}} \tag{43}$$

Therefore, Eq. (43) can be expressed as:

$$\varepsilon_{cu,c} = \left(2 + \frac{\gamma - \gamma_{\min}}{v_{t,eff}}\right)\varepsilon_{c0} \tag{44}$$

in which

$$\gamma = \frac{\varepsilon_{l,j,u}}{\varepsilon_{c0}} = \frac{\varepsilon_{l,i,u}}{k_\varepsilon \varepsilon_{c0}} \tag{45}$$

$$\gamma_{\min} = \frac{\varepsilon_{l1}}{\varepsilon_{c0}} = \frac{2\varepsilon_{c0} c_1 v_{s,\max}}{\varepsilon_{c0}} = 2c_1 v_{s,\max} \tag{46}$$

Since a FRP partially confined concrete with $s_f / D \geq 1$ was assumed behaving almost as an unconfined concrete, in this case, $\varepsilon_{cu,c}$ can be reasonably approximated as $2\varepsilon_{c0}$ (Mander *et al.* (1988)) and according to the proposed $v_s / v_{s,max}$ versus ε_c relation (Fig. 11), $\varepsilon_{l,i,u} = 2k_\varepsilon \varepsilon_{c0} c_1 v_{s,\max}$. Moreover, for $0 < s_f / D \leq 1$, it is assumed that $\varepsilon_{l,i,u}$ linearly decreases from $\varepsilon_{h,rup}$ to $2k_\varepsilon \varepsilon_{c0} c_1 v_{s,\max}$ corresponding to $s_f / D = 0$ and $s_f / D \geq 1$, respectively. Therefore, $\varepsilon_{l,i,u}$ can be estimated as (Fig. 14b):

$$\varepsilon_{l,i,u} = \varepsilon_{h,rup} - \left(\varepsilon_{h,rup} - 2k_\varepsilon \varepsilon_{c0} c_1 v_{s,\max}\right)\left(\frac{s_f}{D}\right) \quad , \quad 2k_\varepsilon \varepsilon_{c0} c_1 v_{s,\max} \leq \varepsilon_{l,i,u} \leq \varepsilon_{h,rup} \tag{47}$$

Simplifying Eq. (47), and then, introducing in Eq. (45), the parameter γ can be determined as:

$$\gamma = \frac{\varepsilon_{l,i,u}}{k_\varepsilon \varepsilon_{c0}} = \left(1 - \frac{s_f}{D}\right)\gamma_{\max} + \frac{s_f}{D}\gamma_{\min} \quad , \quad \gamma_{\min} \leq \gamma \leq \gamma_{\max} \tag{48}$$

in which

$$\gamma_{\max} = \frac{\varepsilon_{h,rup}}{k_\varepsilon \varepsilon_{c0}} = \frac{0.586\beta\varepsilon_{fu}}{k_\varepsilon \varepsilon_{c0}} \tag{49}$$

Therefore, to calculate the ultimate axial strain $\varepsilon_{cu,c}$ corresponding to concrete crushing using Eq. (44), the effective tangential Poisson's ratio of $v_{t,eff}$ should be determined. In the present study, according to the best curve fit of the experimental results of the FRP partially confined specimens with $s_f / D \geq 0.5$ (highly likely to experience concrete crushing prior to FRP rupture, as confirmed by Zeng *et al.* (2018a)), based on a back analysis, $v_{t,eff}$ corresponding to $\varepsilon_{cu,c}$ (Eq. (44)) was proposed as follows:

$$v_{t,eff} = \frac{0.049}{\sqrt{\rho_K}} \tag{50}$$

In Fig. 15a, the experimental results corresponding to the effective tangential Poisson's ratio derived from Eq. (42) are compared with the theoretical counterparts. As can be seen, there is an acceptable predictive performance for the proposed model. As a result, replacing Eq. (50) into Eq. (44) gives:

$$\varepsilon_{cu,c} = \left(2 + 20.4\left(\gamma - \gamma_{\min}\right)\sqrt{\rho_K}\right)\varepsilon_{c0} \tag{51}$$

Using Eq. (51), $\varepsilon_{cu,c}$ corresponding to concrete crushing failure mode can be determined. Fig. 15b demonstrates that Eq. (51) is able to estimate experimental $\varepsilon_{cu,c}$ with acceptable agreement. As a result, based on Eq. (36), when $\varepsilon_c > \varepsilon_{cu}$, the analytical incremental procedure gets terminated by determining failure mode either by FRP rupture or concrete crushing.

Verification

In this section, the reliability of the proposed confinement model for predicting dilation response of fully and partially FRP confined concrete elements of circular cross section is assessed. In Fig. 16, a flowchart for calculating the dilation response of FRP fully and partially confined concrete columns is presented. As can be seen, the lateral strain versus axial strain relation can be easily determined by following the proposed incremental procedure.

Zeng *et al.* (2018a) conducted an experimental study on fully and partially FRP confined circular concrete with different confinement configurations. All specimens had a diameter of 150 mm and a height of 300 mm. The compressive strength of unconfined cylindrical concrete was 23.4 MPa.

The values of thickness, tensile elastic modulus and rupture strain of FRP strips were reported as 0.167 mm, 249.1 GPa and 1.66%, respectively. An example calculation of the dilation behavior, ultimate condition and axial response of the test specimen of S-1-3-25 ($s_f / D = 0.75$, $w_f / D = 0.17$ and $n_f = 1$) is presented as follows:

<u>Dilation response:</u> For this purpose, the value of $v_{s,max}$ as a key parameter in the proposed relation should be computed. Based on Eq. (30), ρ_K should be first determined. It can be calculated by using Eq. (27) as:

$$\rho_K = \frac{1}{2} K_e \frac{\rho_f E_f}{f_{c0}/\varepsilon_{c0}} = 0.5 \times 0.178 \times \frac{0.0008 \times 249100}{23.4/0.0018} = 0.0014$$

in which

$$K_e = 0.75 + 0.12 \frac{w_f}{D} - 0.79 \frac{s_f}{D} = 0.75 + 0.12 \times 0.17 - 0.79 \times 0.75 = 0.178 \quad \text{(Eq. (20))}$$

$$\rho_f = \frac{4 n_f t_f w_f}{D\left(w_f + s_f\right)} = \frac{4 \times 1 \times 0.167 \times 25}{150\left(25 + 112.5\right)} = 0.0008 \quad \text{(Eq. (23))}$$

$$\varepsilon_{c0} = 0.0015 + \frac{f_{c0}}{70000} = 0.0015 + \frac{23.4}{70000} = 0.0018 \quad \text{(Eq. (28))}$$

Accordingly, introducing ρ_K into Eq. (30), $v_{s,max}$ corresponding to $\varepsilon_{c,m}$ (Eq. (31)) can be calculated as:

$$v_{s,\max} = \frac{0.155}{\left(1.23 - 0.003 f_{c0}\right)\sqrt{\rho_K}} = \frac{0.155}{\left(1.23 - 0.003 \times 23.4\right)\sqrt{0.0014}} = 3.57$$

$$\varepsilon_{c,\mathrm{m}} = 0.0085 - 0.05 \rho_K = 0.0085 - 0.05 \times 0.0014 = 0.0084$$

Accordingly, the relation between $v_s / v_{s,max}$ and ε_c can be calculated as shown in Fig. 1**7**a.

<u>Ultimate conditions:</u> To estimate ultimate axial strain of the test specimens, $\varepsilon_{cu,c}$ and $\varepsilon_{cu.r}$ corresponding to concrete crushing and FRP rupture should be determined by using Eq. (39) and Eq. (51), respectively:

$$\varepsilon_{cu,r} = \frac{\varepsilon_{h,rup}}{k_\varepsilon v_{s,u}} = \frac{0.0107}{0.31 \times v_{s,u}} = \frac{0.0345}{v_{s,u}} \quad \text{(Eq. (39))}$$

$$\varepsilon_{cu,c} = \left(2 + 20.4\left(\gamma - \gamma_{\min}\right)\sqrt{\rho_K}\right)\varepsilon_{c0} = \left(2 + 20.4\left(8.75 - 5.35\right)\sqrt{0.0014}\right)0.0018 = 0.0084 \quad \text{(Eq. (51))}$$

in which

$$\gamma = \left(1 - \frac{s_f}{D}\right)\gamma_{\max} + \frac{s_f}{D}\gamma_{\min} = \left(1 - 0.75\right) \times 18.81 + 0.75 \times 5.39 = 8.75 \qquad \text{(Eq. (45))}$$

$$\gamma_{\min} = 2c_1 v_{s,\max} = 2\left(0.75 + 3.85\rho_K\right)v_{s,\max} = 2 \times \left(0.75 + 3.85 \times 0.0014\right) \times 3.57 = 5.39 \qquad \text{(Eq. (46))}$$

$$\gamma_{\max} = \frac{\varepsilon_{h,rup}}{k_\varepsilon \varepsilon_{c0}} = \frac{0.0107}{0.31 \times 0.0018} = 18.81 \qquad \text{(Eq. (49))}$$

$$\varepsilon_{h,rup} = 0.586\beta\varepsilon_{fu} = \frac{0.586}{0.82 + 0.23\varepsilon_{fu} f_{c0}}\varepsilon_{fu} = \frac{0.586}{0.82 + 0.23 \times 0.0166 \times 23.4} 0.0166 = 0.0107 \quad \text{(Eq. (40))}$$

$$k_\varepsilon = 1 - 0.92\frac{s_f}{D} = 1 - 0.92 \times 0.75 = 0.31 > 0.08 \qquad \text{(Eq. (3))}$$

By drawing the relation between $v_{s,u} / v_{s,max}$ and ε_c, as illustrated in Fig. 17b, $\varepsilon_{cu,r}$ corresponding to FRP rupture is obtained as 0.0101. As a result, based on Eq. (35), comparing $\varepsilon_{cu,c}$ and $\varepsilon_{cu,r}$, ultimate axial strain ε_{cu} is equal to 0.0084 with concrete crushing failure mode.

Fig. 18 compares the dilation responses of the test specimens with different configurations reported by Zeng *et al.* (2018a) with those obtained from the proposed model. As can be observed, the good predictive performance of the model confirms the reliability and efficiency of the proposed analytical model to predict lateral strain versus axial strain curves, working for both FRP fully and partially confined circular concrete.

Lim and Ozbakkaloglu (2014c) experimentally investigated the effects of concrete compressive strength and the type of FRP materials (CFRP, GFRP and AFRP) on the axial and dilation behavior of FRP fully confined concrete columns of circular cross section. All specimens had a diameter of 152 mm with a height of 305 mm. Four different values of f_{c0} were considered equal to 30, 50, 74 and 98 MPa. The values of FRP thickness, tensile elastic modulus and rupture strain were reported as 0.2 mm, 128.5 GPa and 1.86%; 0.165 mm, 236 GPa and 1.76%; and 0.2 mm, 95.3 GPa and 3.21%; for AFRP, CFRP and GFRP, respectively. The details of the experimental program can be found from Lim and Ozbakkaloglu (2014c). In Fig. 19, the dilation responses registered experimentally and obtained from the proposed model are compared. As can be seen, in general, the proposed model is able to sufficiently predict the experimental counterparts in case of full confinement with various the types of FRP material and f_{c0}.

To extensively verify the proposed confinement model, dilation responses of test specimens with partial confinement conducted by Barros and Ferreira (2008), Zeng *et al.* (2017 and 2018b) are also compared in Fig. 20 to those obtained with the developed model. Overall, a good predictive performance confirms the reliability and efficiency of the proposed analytical model to predict the lateral strain versus axial strain of FRP partially confined concrete elements of circular cross section.

Summary and conclusions

In this study, a new model was developed to predict dilation behavior of fully and partially FRP confined concrete elements of circular cross section. To estimate dilation response, the secant Poisson's ratio versus axial strain relations at the critical section placed at the middle distance between FRP strips and at the mid-plane of the strips were proposed as a function of confinement stiffness for full and partial confinement arrangements. To simulate the concrete columns with partial confinement configurations, the confinement stiffness index proposed by Teng *et al.* (2009) was modified based on the concept of confinement efficiency factor. For this purpose, in addition to vertical arching action, the effect of the non-uniform distribution of the concrete expansion was addressed for determining the confinement efficiency factor. A new methodology was also developed to predict the ultimate condition of partially FRP confined concrete taking into account the possibility of concrete crushing and FRP rupture failure modes. To validate the analytical model, it was vastly applied to predict the dilation behavior of the relevant experimental specimens available in the literature. The comparison between the model and experimental counterparts revealed that it is capable of providing an estimation of dilation responses with appropriate precision for design purposes.

Acknowledgments

This study is a part of the project ‘‘StreColesf_Innovative technique using effectively composite materials for the strengthening of rectangular cross section reinforced concrete columns exposed to seismic loadings and fire’’, with the reference POCI-01-0145-FEDER-029485.

Data Availability Statement

All data, models, and code generated or used during the study appear in the submitted article.

References

Al-Salloum, Y. A. (2007). "Influence of edge sharpness on the strength of square concrete columns confined with FRP composite laminates." Composites Part B: Engineering, 38(5-6), 640-650.

ACI Committee (2008). "ACI 440.2R-08: Guide for the design and construction of externally bonded FRP systems for strengthening concrete structures." American Concrete Institute, Farmington Hills, Michigan, 38.

Barros, J. A., and Ferreira, D. R. (2008). "Assessing the efficiency of CFRP discrete confinement systems for concrete cylinders." Journal of Composites for Construction, 12(2), 134-148.

Benzaid, R., and Mesbah, H. A. (2013). "Circular and square concrete columns externally confined by CFRP composite: experimental investigation and effective strength models." Fiber Reinforced Polymers–The Technology Applied for Concrete Repair, 167-201.

Berthet, J., Ferrier, E., and Hamelin, P. (2005). "Compressive behavior of concrete externally confined by composite jackets. Part A: experimental study." Construction and Building Materials, 19(3), 223-232.

Candappa, D., Sanjayan, J., and Setunge, S. (2001). "Complete triaxial stress-strain curves of high-strength concrete." Journal of Materials in Civil Engineering, 13(3), 209-215.

CNR-DT 200 (2004). "Guide for the design and construction of externally bonded FRP systems for strengthening existing structures." Italian National Research Council.

Eid, R., Roy, N., and Paultre, P. (2009). "Normal-and high-strength concrete circular elements wrapped with FRP composites." Journal of Composites for Construction, 13(2), 113-124.

Fib Bulletin 14. (2001). "Externally bonded FRP reinforcement for RC structures." International Federation for Structural Concrete.

Guo, Y.-C., Gao, W.-Y., Zeng, J.-J., Duan, Z.-J., Ni, X.-Y., and Peng, K.-D. (2019). "Compressive behavior of FRP ring-confined concrete in circular columns: Effects of specimen size and a new design-oriented stress-strain model." Construction and Building Materials, 201, 350-368.

Guo, Y.-C., Xiao, S.-H., Luo, J.-W., Ye, Y.-Y., and Zeng, J.-J. (2018). "Confined concrete in fiber-reinforced polymer partially wrapped square columns: axial compressive behavior and strain distributions by a particle image velocimetry sensing technique." Sensors, 18(12), 4118.

Huang, L., Gao, C., Yan, L., Kasal, B., Ma, G., and Tan, H. (2016). "Confinement models of GFRP-confined concrete: Statistical analysis and unified stress–strain models." Journal of Reinforced Plastics and Composites, 35(11), 867-891.

Janwaen, W., Barros, J. A., and Costa, I. G. (2019). "A new strengthening technique for increasing the load carrying capacity of rectangular reinforced concrete columns subjected to axial compressive loading." Composites Part B: Engineering, 158, 67-81.

Karthik, M. M., and Mander, J. B. (2011). "Stress-block parameters for unconfined and confined concrete based on a unified stress-strain model." Journal of Structural Engineering, 137(2), 270-273.

Lam, L., and Teng, J. (2003). "Design-oriented stress–strain model for FRP-confined concrete." Construction and Building Materials, 17(6-7), 471-489.

Lim, J. C., and Ozbakkaloglu, T. (2014a). "Lateral strain-to-axial strain relationship of confined concrete." Journal of Structural Engineering, 141(5), 04014141.

Lim, J. C., and Ozbakkaloglu, T. (2014b). "Unified stress-strain model for FRP and actively confined normal-strength and high-strength concrete." Journal of Composites for Construction, 19(4), 04014072.

Lim, J. C., and Ozbakkaloglu, T. (2014c). "Hoop strains in FRP-confined concrete columns: experimental observations." Materials and Structures, 48(9), 2839-2854.

Mai, A. D., Sheikh, M. N., and Hadi, M. N. "Influence of the location of CFRP strips on the behaviour of partially wrapped square reinforced concrete columns under axial compression." Proc., Structures, Elsevier, 131-137.

Mander, J. B., Priestley, M. J., and Park, R. (1988). "Theoretical stress-strain model for confined concrete." Journal of Structural Engineering, 114(8), 1804-1826.

Mirmiran, A., and Shahawy, M. (1997). "Dilation characteristics of confined concrete." Mechanics of Cohesive- frictional Materials: An International Journal on Experiments, Modelling and Computation of Materials and Structures, 2(3), 237-249.

Osorio, E., Bairán, J. M., and Marí, A. R. (2013). "Lateral behavior of concrete under uniaxial compressive cyclic loading." Materials and Structures, 46(5), 709-724.

Ozbakkaloglu, T., Lim, J. C., and Vincent, T. (2013). "FRP-confined concrete in circular sections: Review and assessment of stress–strain models." Engineering Structures, 49, 1068-1088.

Perrone, M., Barros, J. A., and Aprile, A. (2009). "CFRP-based strengthening technique to increase the flexural and energy dissipation capacities of RC columns." Journal of Composites for Construction, 13(5), 372-383.

Rochette, P., and Labossiere, P. (2000). "Axial testing of rectangular column models confined with composites." Journal of Composites for Construction, 4(3), 129-136.

Shayanfar, J., and Bengar, H. A. (2018). "A practical model for simulating nonlinear behaviour of FRP strengthened RC beam-column joints." Steel and Composite Structures, 27(1), 49-74.

Shehata, I. A., Carneiro, L. A., and Shehata, L. C. (2002). "Strength of short concrete columns confined with CFRP sheets." Materials and Structures, 35(1), 50-58.

Suon, S., Saleem, S., and Pimanmas, A. (2019). "Compressive behavior of basalt FRP-confined circular and non-circular concrete specimens." Construction and Building Materials, 195, 85-103.

Tamuzs, V., Tepfers, R., Zile, E., and Ladnova, O. (2006). "Behavior of concrete cylinders confined by a carbon composite 3. Deformability and the ultimate axial strain." Mechanics of Composite Materials, 42(4), 303-314.

Teng, J., Jiang, T., Lam, L., and Luo, Y. (2009). "Refinement of a design-oriented stress–strain model for FRP-confined concrete." Journal of Composites for Construction, 13(4), 269-278.

Teng, J., Huang, Y., Lam, L., and Ye, L. (2007). "Theoretical model for fiber-reinforced polymer-confined concrete." Journal of Composites for Construction, 11(2), 201-210.

Teng, J., and Lam, L. (2002). "Compressive behavior of carbon fiber reinforced polymer-confined concrete in elliptical columns." Journal of Structural Engineering, 128(12), 1535-1543.

Vincent, T., and Ozbakkaloglu, T. (2015). "Compressive behavior of prestressed high-strength concrete-filled aramid FRP tube columns: Experimental observations." Journal of Composites for Construction, 19(6), 04015003.

Wang, W., Sheikh, M. N., Al-Baali, A. Q., and Hadi, M. N. (2018). "Compressive behaviour of partially FRP confined concrete: Experimental observations and assessment of the stress-strain models." Construction and Building Materials, 192, 785-797.

Wang, L.-M., and Wu, Y.-F. (2008). "Effect of corner radius on the performance of CFRP-confined square concrete columns: Test." Engineering Structures, 30(2), 493-505.

Xiao, Y., and Wu, H. (2003). "Compressive behavior of concrete confined by various types of FRP composite jackets." Journal of Reinforced Plastics and Composites, 22(13), 1187-1201.

Zeng, J.-J., Guo, Y.-C., Gao, W.-Y., Chen, W.-P., and Li, L.-J. (2018a). "Stress-strain behavior of concrete in circular concrete columns partially wrapped with FRP strips." Composite Structures, 200, 810-828.

Zeng, J., Guo, Y., Li, L., and Chen, W. (2018b). "Behavior and three-dimensional finite element modeling of circular concrete columns partially wrapped with FRP strips." Polymers, 10(3), 253.

Zeng, J.-J., Guo, Y.-C., Gao, W.-Y., Li, J.-Z., and Xie, J.-H. (2017). "Behavior of partially and fully FRP-confined circularized square columns under axial compression." Construction and Building Materials, 152, 319-332.

TABLES

List of Tables:

FIGURES

List of Figures:

Table 1

Table 1. Details of the test specimens

ID		s_f / D	f_{cc}^{exp} / f_{c0}	$v'_{s,u}{}^{exp}$	$k_\varepsilon^{exp\ a}$
Barros and Ferreira (2008)	**W15S3L1**	**0.57**	1.01	0.82	**0.33**
	W15S3L2	**0.57**	1.01	0.74	**0.29**
	W15S3L3	**0.57**	1.01	1.05	**0.42**
	W15S3L4	**0.57**	1.04	0.89	**0.36**
Zeng *et al.* (2018a)	**S-1-3-25-1**	**0.75**	1.09	0.92	**0.37**
	S-1-3-25-2	**0.75**	1.10	0.98	**0.39**
	S-1-3-30-1	**0.70**	1.09	0.98	**0.39**
	S-1-3-30-2	**0.70**	1.08	1.05	**0.42**
	S-1-3-35-1	**0.65**	1.16	0.85	**0.34**
	S-1-3-35-2	**0.65**	1.07	1.06	**0.42**
	S-2-3-25-1	**0.75**	1.15	0.95	**0.38**
	S-2-3-25-2	**0.75**	1.17	0.98	**0.39**
	S-1-4-25-1	**0.44**	1.13	1.19	**0.47**
	S-1-4-25-2	**0.44**	1.16	1.29	**0.52**
Zeng *et al.* (2018b)	**S-1-3-25**	**0.75**	1.00	1.31	**0.52**
	S-1-3-30	**0.73**	1.00	1.54	**0.62**
	S-1-4-25	**0.44**	1.05	1.14	**0.45**
Wang *et al.* (2018)	**S75**	**0.75**	1.23	0.67	**0.27**
	S100	**1.00**	1.18	0.24	**0.10**
	S150	**1.50**	1.11	0.24	**0.10**

Note: [a]: $k_\varepsilon^{\mathrm{exp}} = v'_{s,u}{}^{\mathrm{exp}} / 2.5$

Table 2

Table 2. Assembled database for fully and partially FRP confined concrete elements of circular cross section

ID	Confinement arrangement			f_{c0} (MPa)	ρ_K (%)	$v_{s,max}$
	Total number	Full	Partial			
Rochette and Labossie`re (2000)	2	2	-	42.0 – 43.0	3.4 – 5.0	0.61 – 0.97
Shehata *et al.* (2001)	2	2	-	25.6 – 29.8	3.8 – 6.7	0.76 – 0.87
Teng and Lam (2002)	3	3	-	36.6 – 39.0	2.2 – 4.4	0.66 – 0.99
Xiao and Wu (2003)	39	39	-	34.5 – 57.0	2.1 – 9.3	0.32 – 1.50
Berthet *et al*. (2005)	15	15	-	22.2 – 171	2.0 – 15.1	0.65 – 2.08
Al-Salloum (2007)	1	1	-	28.8	8.0	0.64
Barros and Ferreira (2008)	39	8	31	22.9 – 40.0	0.2 – 26.2	0.25 – 2.20
Wang and Wu (2008)	4	4	-	30.9 – 52.1	2.1 – 6.1	0.62 – 1.98
Eid *et al.* (2009)	18	18	-	31.1 – 75.9	1.3 – 6.9	0.45 – 1.29
Benzaid and Mesbah (2014)	6	6	-	25.9 – 61.8	1.6 – 9.2	0.95 – 3.77
Lim and Ozbakkaloglu (2014c)	36	36	-	29.6 – 98.0	1.6 – 6.1	0.61 – 1.53
Vincent and Ozbakkaloglu (2015)	6	6	-	110.3	3.8 – 5.7	0.77 - 1.06
Zeng *et al.* (2017)	12	3	9	24.3	0.8 – 8.3	0.62 – 1.84
Zeng *et al.* (2018a)	57	6	54	23.4	0.2 - 13	0.39 - 3.16
Zeng *et al.* (2018b)	15	-	15	23.5	0.2 – 5.6	0.90 – 5.31
Wang *et al.* (2018)	7	1	6	36.0	0.3 - 5.9	0.42 – 3.03
Guo *et al.* (2019)	21	-	21	33.6 – 41.7	0.5 – 5.0	0.44 – 1.73
Suon *et al.* (2019)	3	3	-	15.8	1.4 - 4.2	1.00 – 1.53
ALL	**289**	**153**	**136**	**15.8-171**	**0.2-26.2**	**0.2-5.3**

Table 3

Table 3. Comparison of the reliability of the proposed model and other models

ID	Expression	Mean	SD	MAPE
Lam and Teng (2003) ACI 440.2R-08 (2008)	$\frac{\varepsilon_{h,rup}}{\varepsilon_{fu}} = 0.586$	1.03	0.68	0.33
Lim and Ozbakkaloglu (2014b)	$\frac{\varepsilon_{h,rup}}{\varepsilon_{fu}} = 0.9 - 0.0023 f_{c0} - 0.75 E_f \times 10^{-6}$	1.19	0.80	0.38
Proposed model	$\frac{\varepsilon_{h,rup}}{\varepsilon_{fu}} = 0.586\beta$ in which $\beta = \frac{1}{0.82 + 0.23\varepsilon_{fu} f_{c0}}$	1.00	0.63	0.31

Figure 1

Click here to access/download;Figure;Fig 1.pdf

Fig. 1

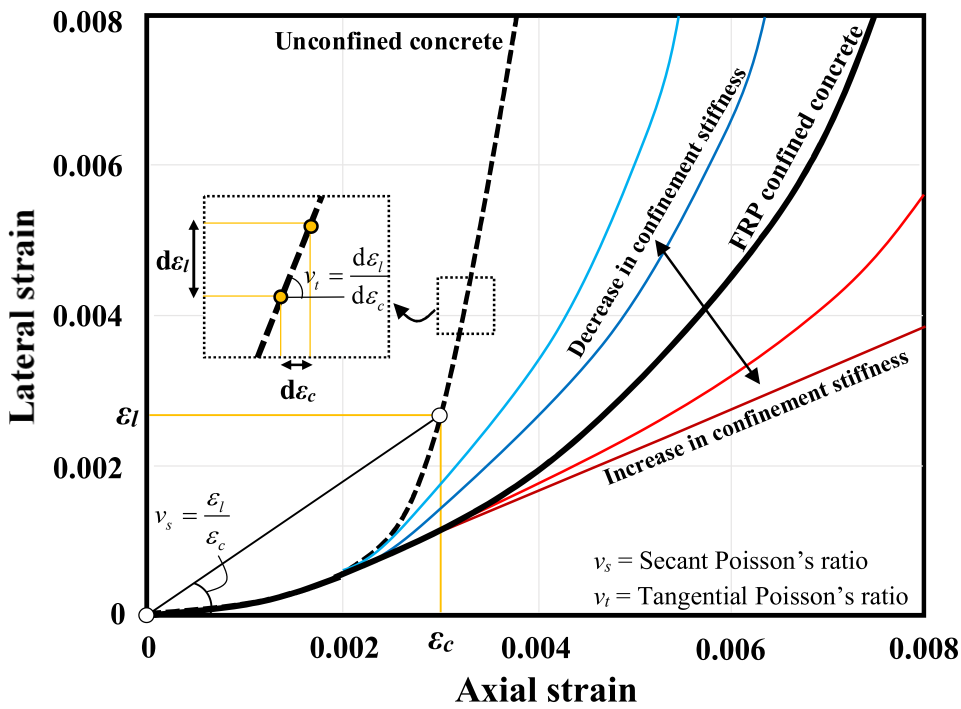

Fig. 1. Dilation behavior of typical FRP confined concrete

Fig. 2

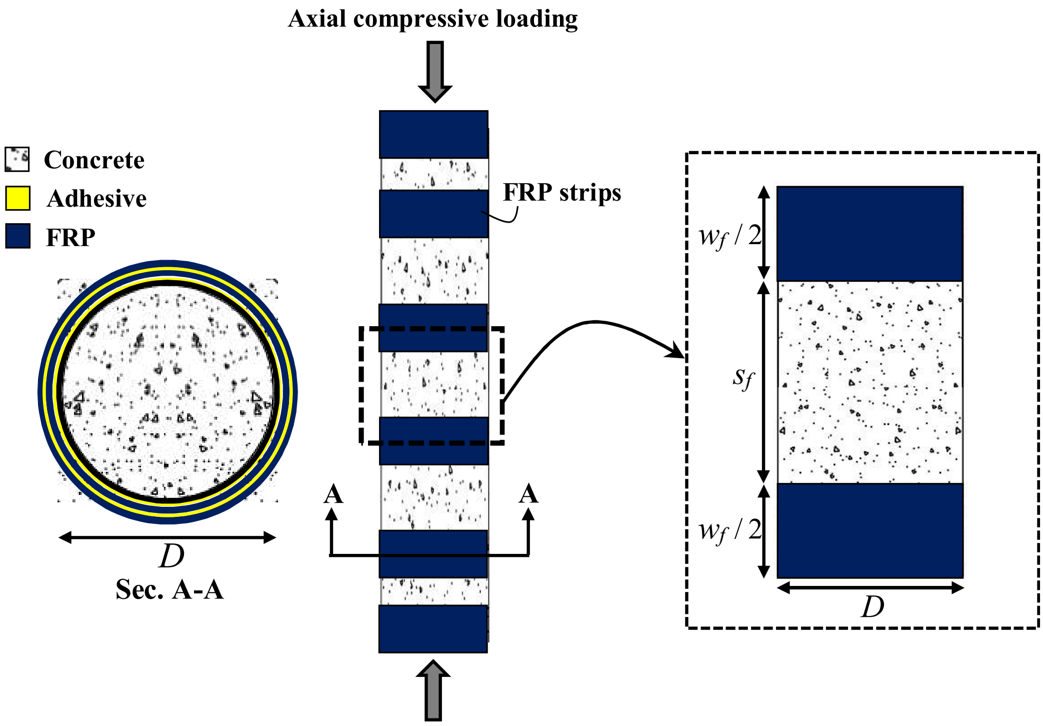

Fig. 2. Detailing of concrete column partially confined by FRP strips

Fig. 3

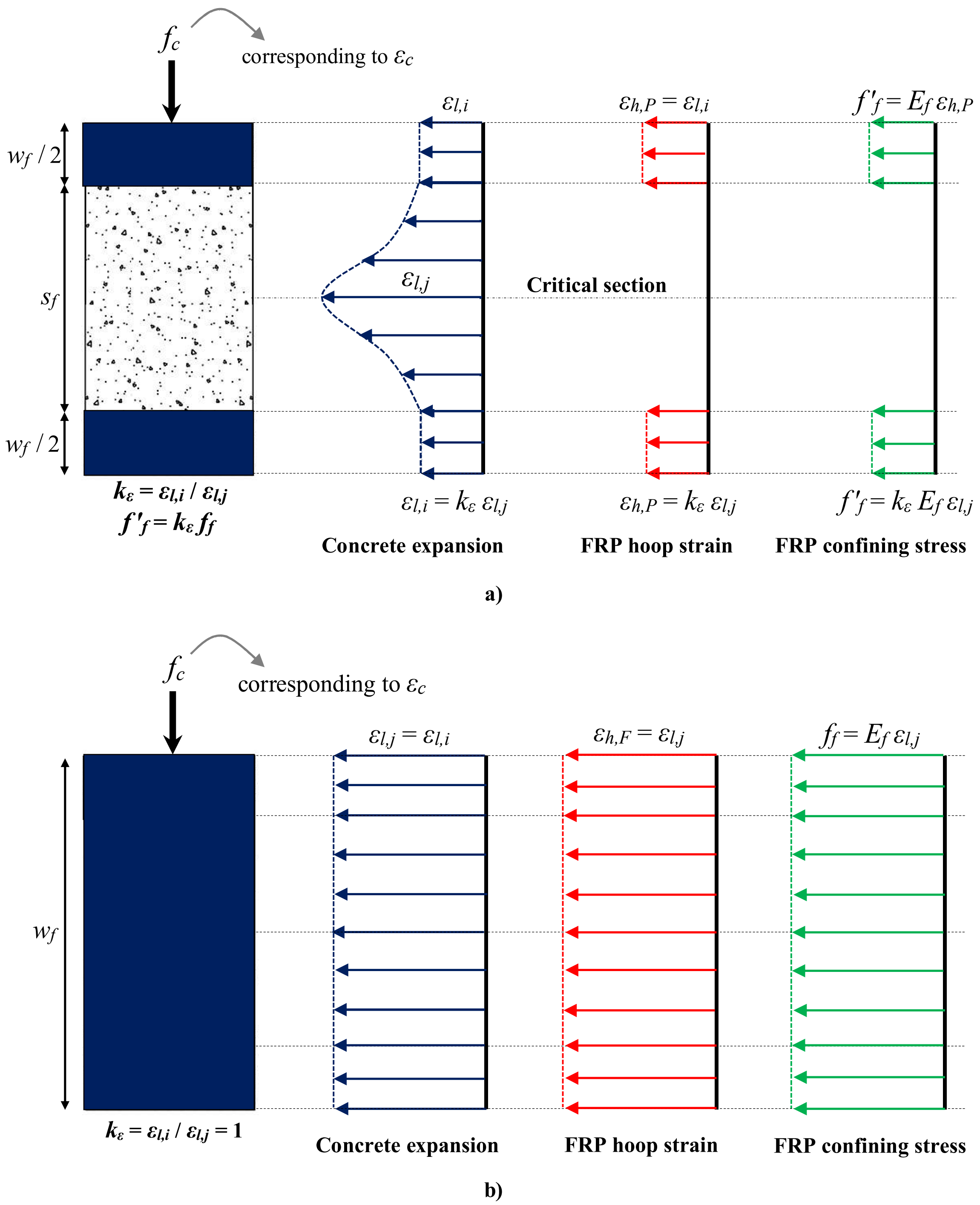

Fig. 3. Lateral expansion in FRP confined concrete: a) partial confinement and b) full confinement

Fig. 4

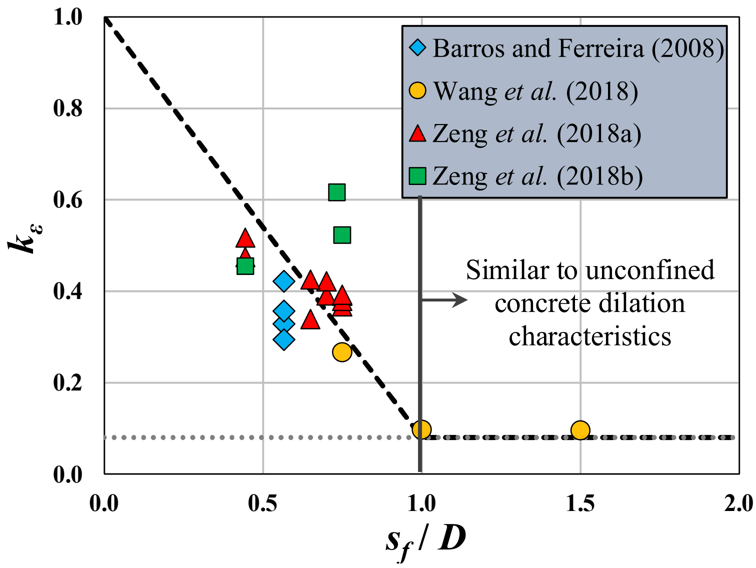

Fig. 4. Variation of k_ε with s_f obtained from Eq. (3) and the experimental results reported by Barros and Ferreira (2008), Wang *et al.* (2018), Zeng *et al.* (2018a and 2018b)

Fig. 5

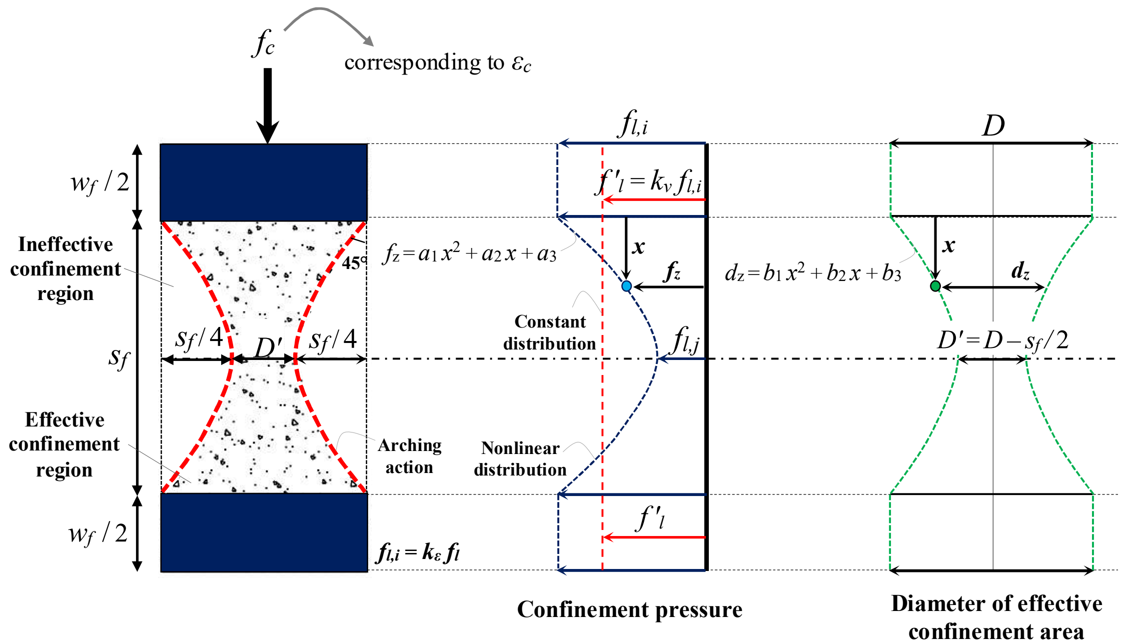

a)

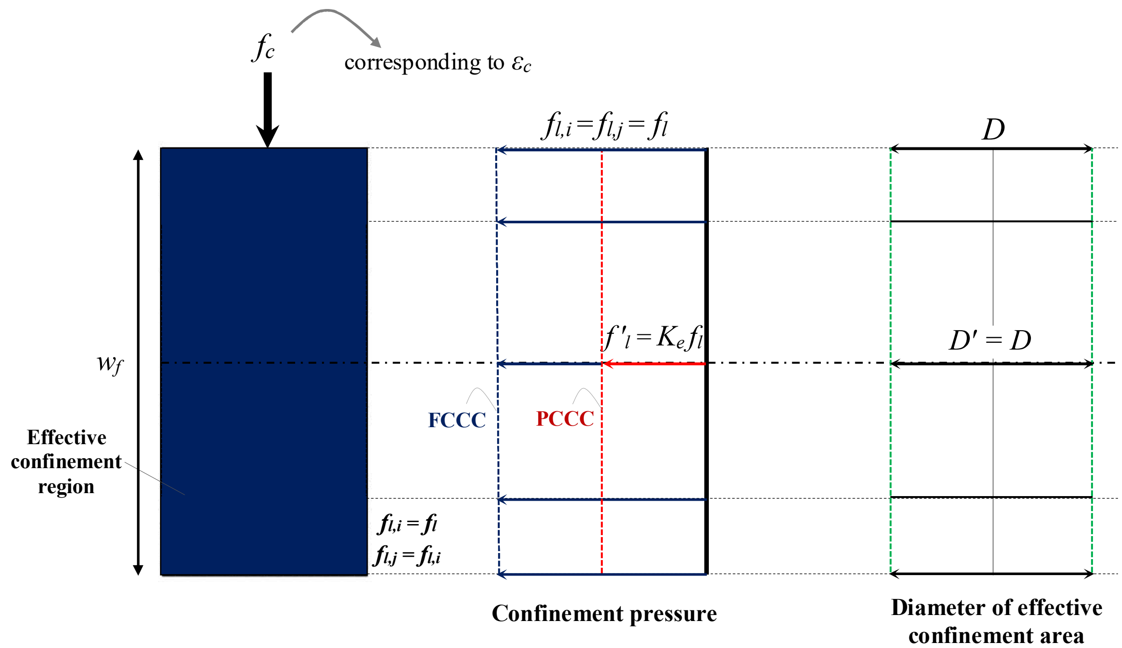

b)

Fig. 5. FRP confined concrete with a) partial confinement b) full confinement

Note: FCCC and PCCC denote fully and partially confined concrete columns of circular cross section, respectively

Fig. 6

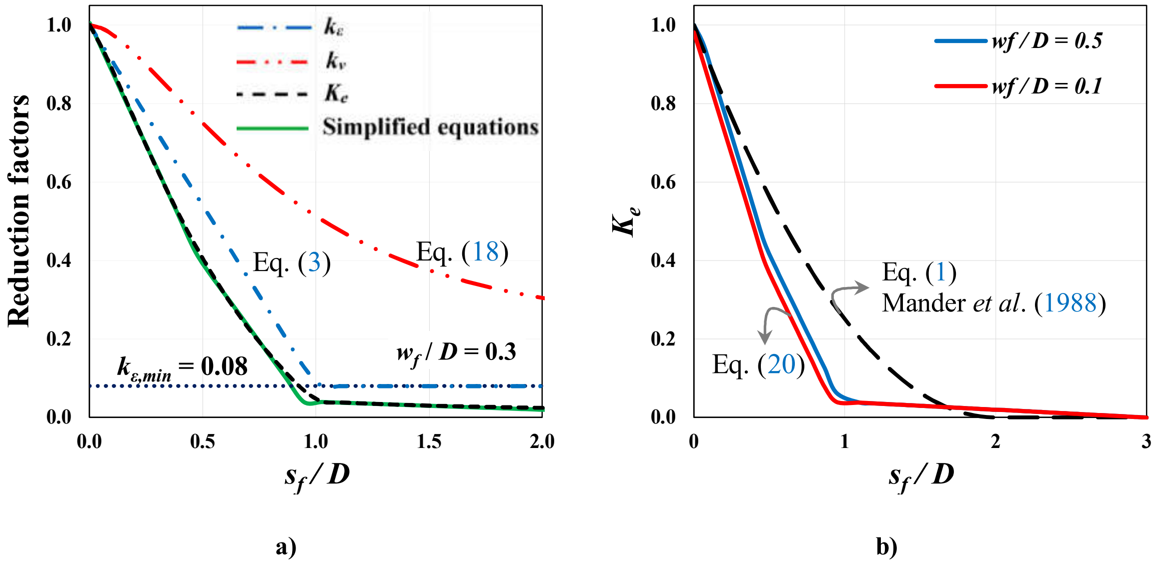

Fig. 6. Variation of K_e with s_f / D for a partial system

Fig. 7

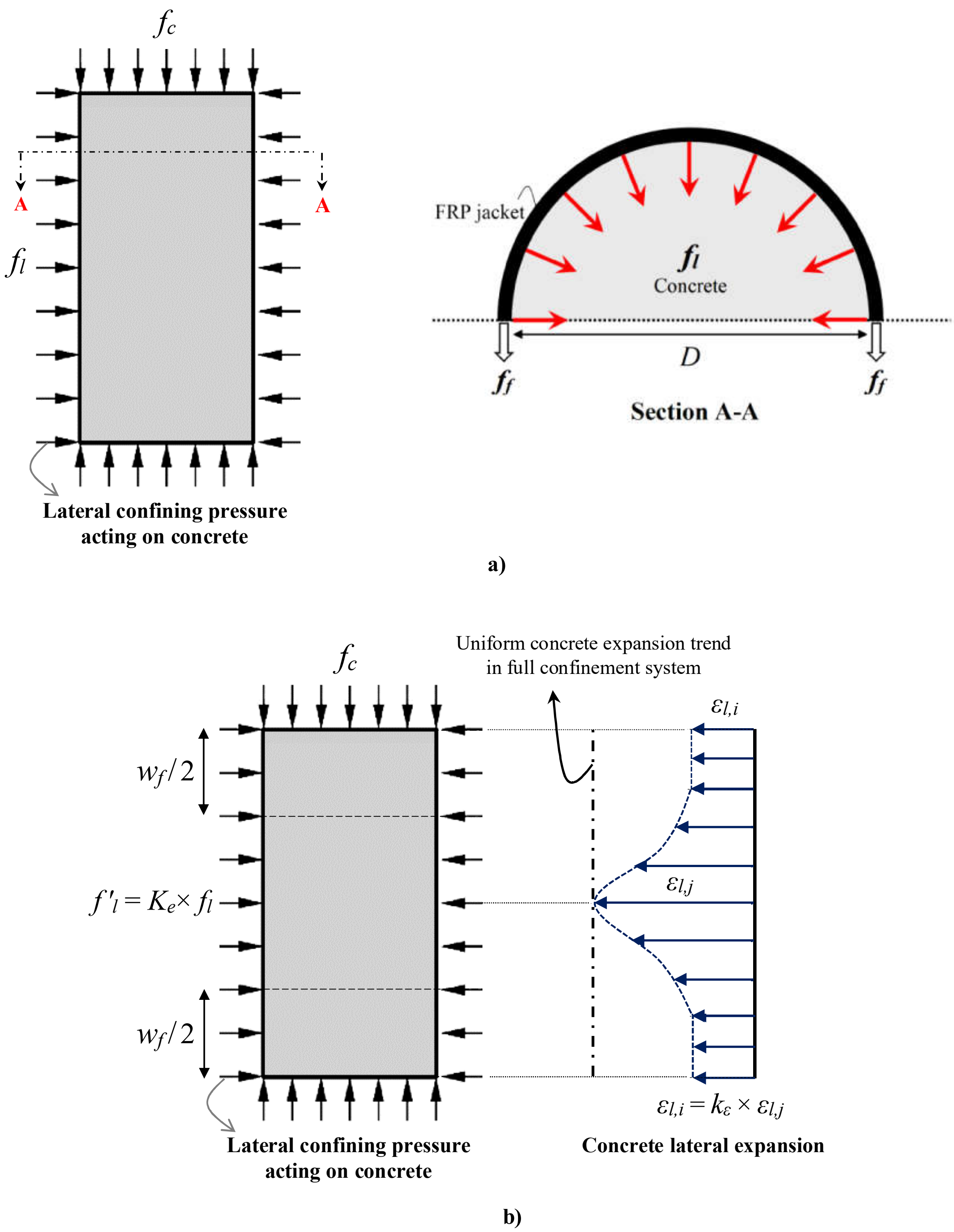

Fig. 7. Confining action in FRP confined concrete columns; a) full confinement mechanism, b) partial confinement mechanism

Figure 8

Click here to access/download;Figure;Fig 8.pdf

Fig. 8

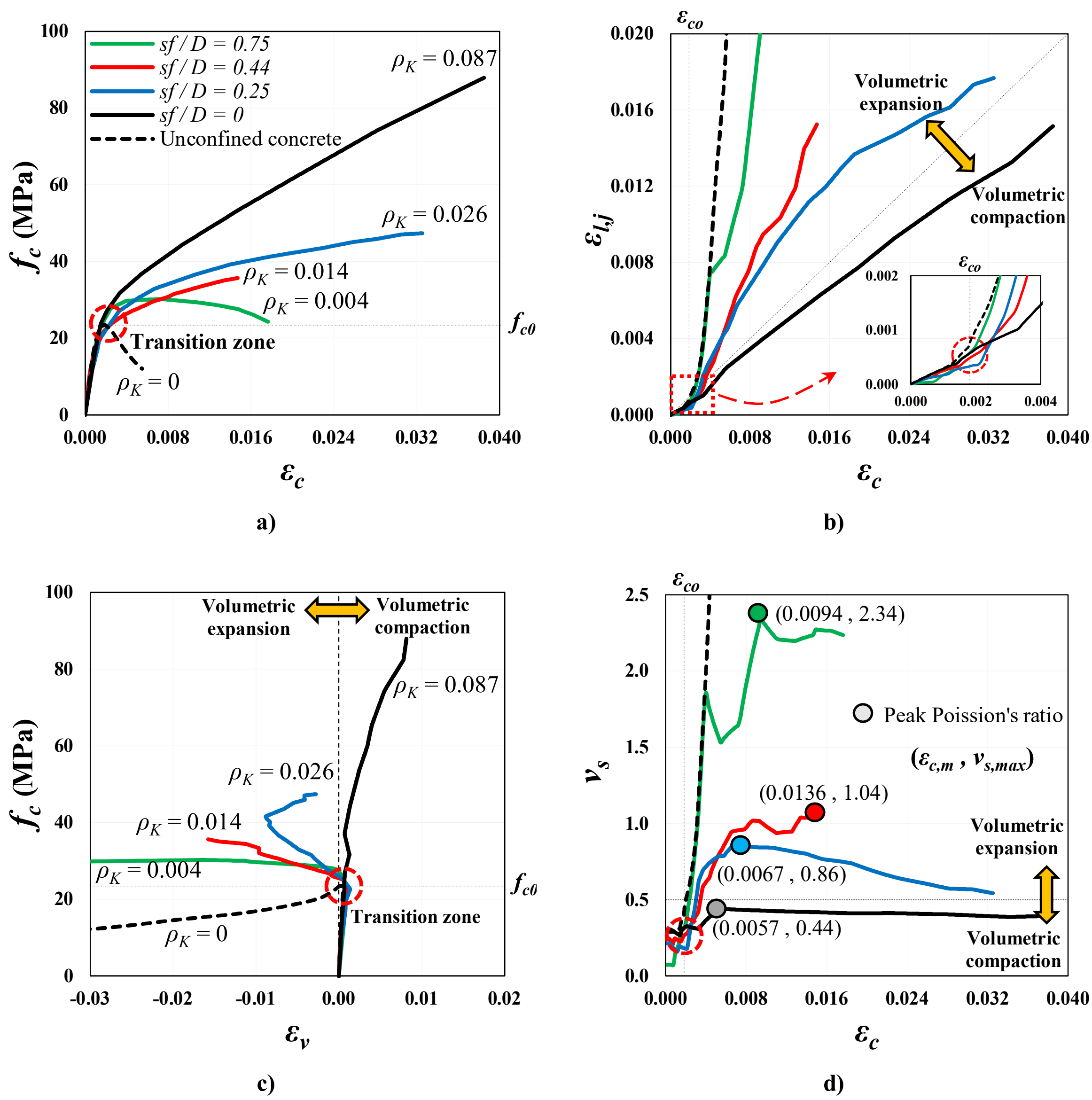

Fig. 8. Axial and lateral behavior for the test specimens with two FRP layers, conducted by Zeng *et al.* (2018a): a) axial stress *vs* axial strain curve; b) concrete lateral strain *vs* axial strain curve; c) axial stress *vs* volumetric strain; d) secant Poisson's ratio *vs* axial strain

Fig. 9

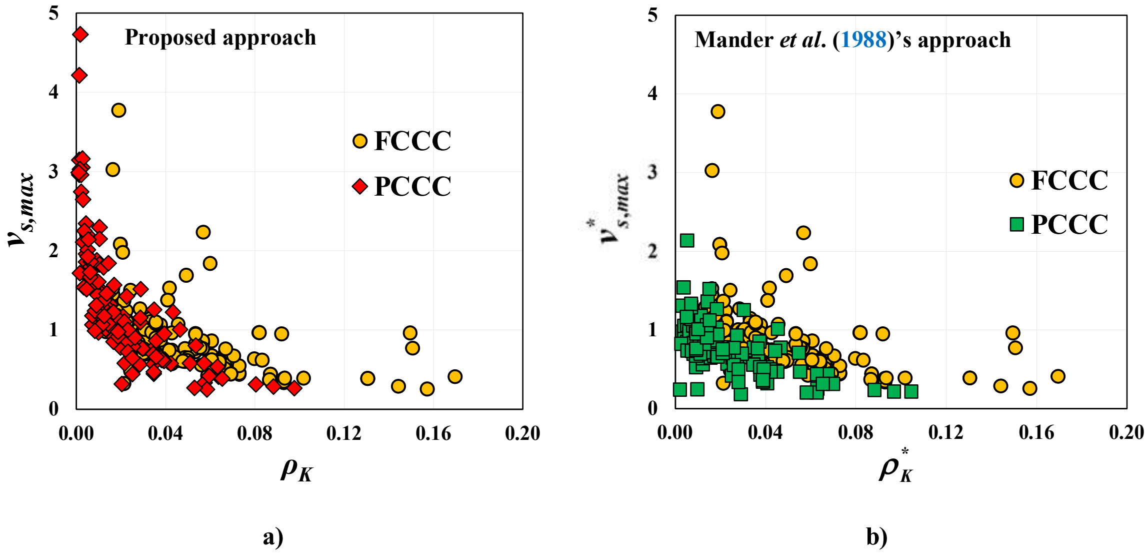

Fig. 9. Variation of experimental dilation results with confinement stiffness index: a) proposed approach, b) Mander *et al.* (1988)'s approach

(FCCC: Fully confined concrete column of circular cross section; PCCC: Partially confined concrete column of circular cross section)

Fig. 10

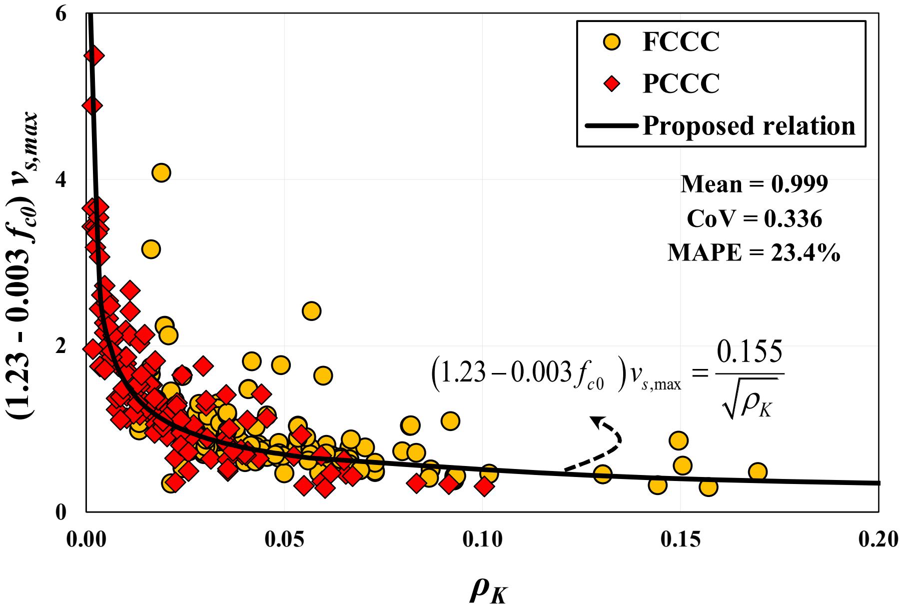

Fig. 10. Variations of the experimental $v_{s,max}$ as a function of ρ_K

Fig. 11

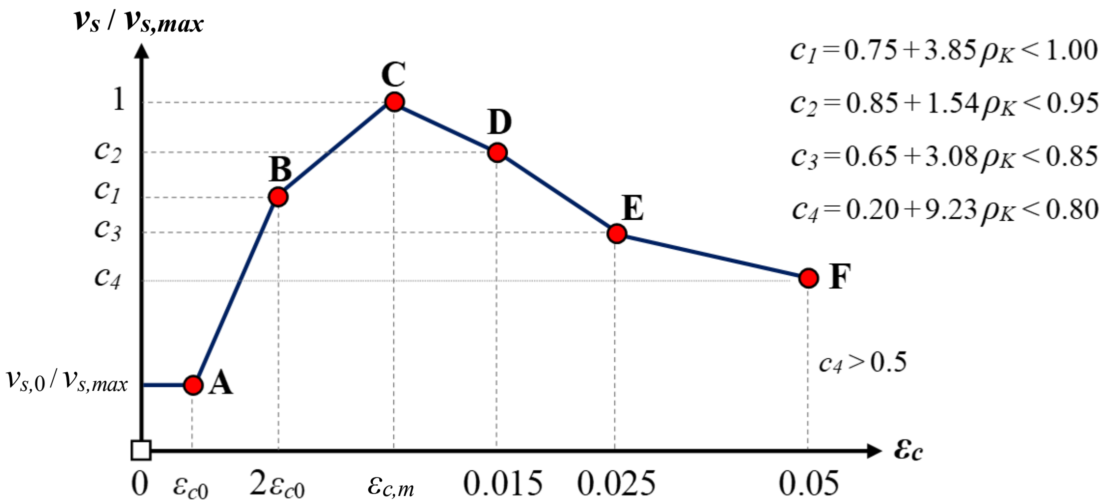

Fig. 11. Normalized secant Poisson's ratio versus axial strain as a function of ρ_K

Fig. 12

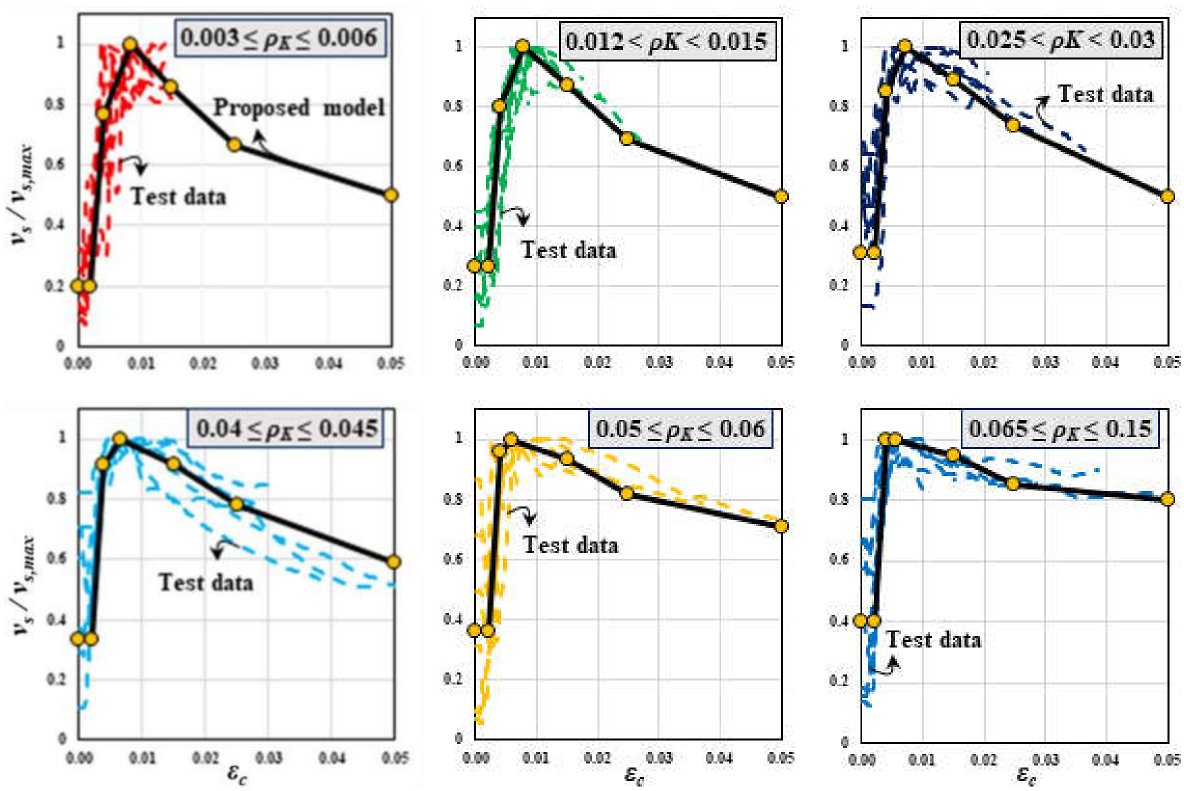

Fig. 12. Comparison of the proposed analytical relation and experimental results for the different levels of ρ_K

Note: Experimental results were reported by Teng and Lam (2002), Berthet *et al.* (2005); Eid *et al.* (2009), Benzaid and Mesbah (2014); Vincent and Ozbakkaloglu (2015), Zeng *et al.* (2018a), Zeng *et al.* (2018b), Guo *et al.* (2019) and Suon *et al.* (2019)

Fig. 13

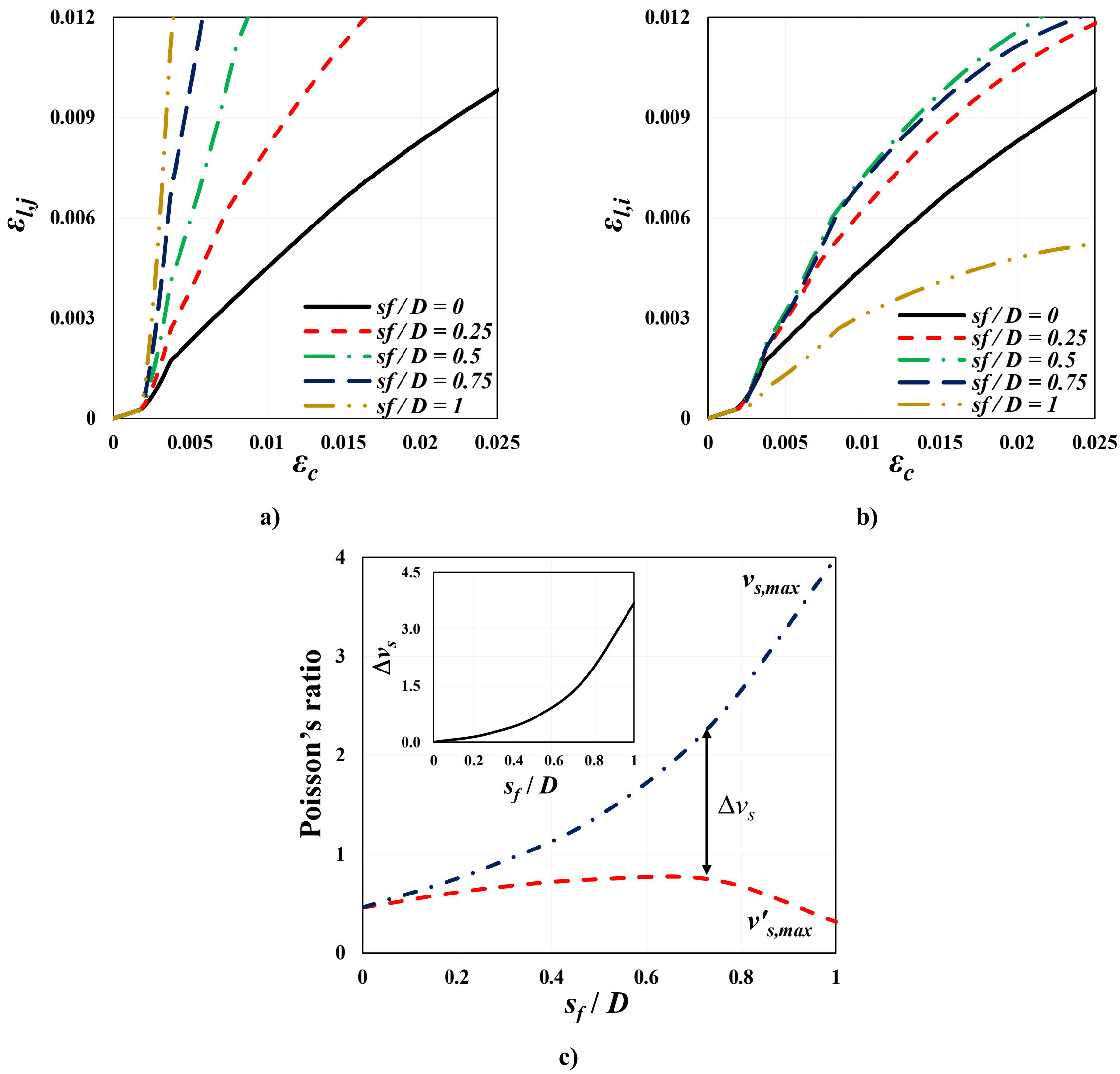

Fig. 13. a) and b) Variations of $\varepsilon_{l,j}$ and $\varepsilon_{l,i}$ with ε_c ; c) influence of s_f / D on $v_{s,max}$ and $v'_{s,max}$

Fig. 14

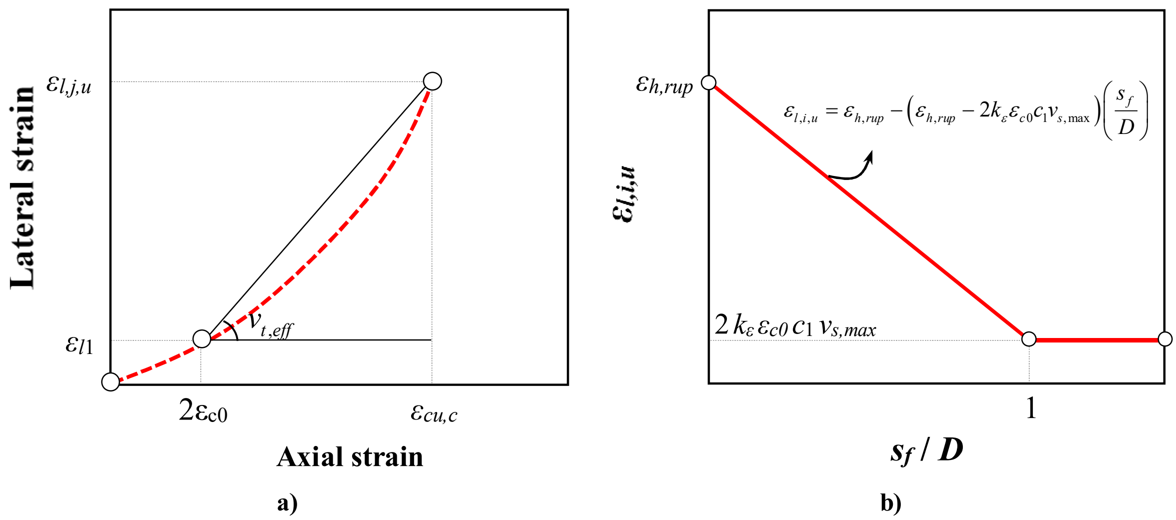

Fig. 14. a) Typical lateral versus axial strain curve; b) Typical $\varepsilon_{l,i,u}$ versus s_f / D curve

Fig. 15

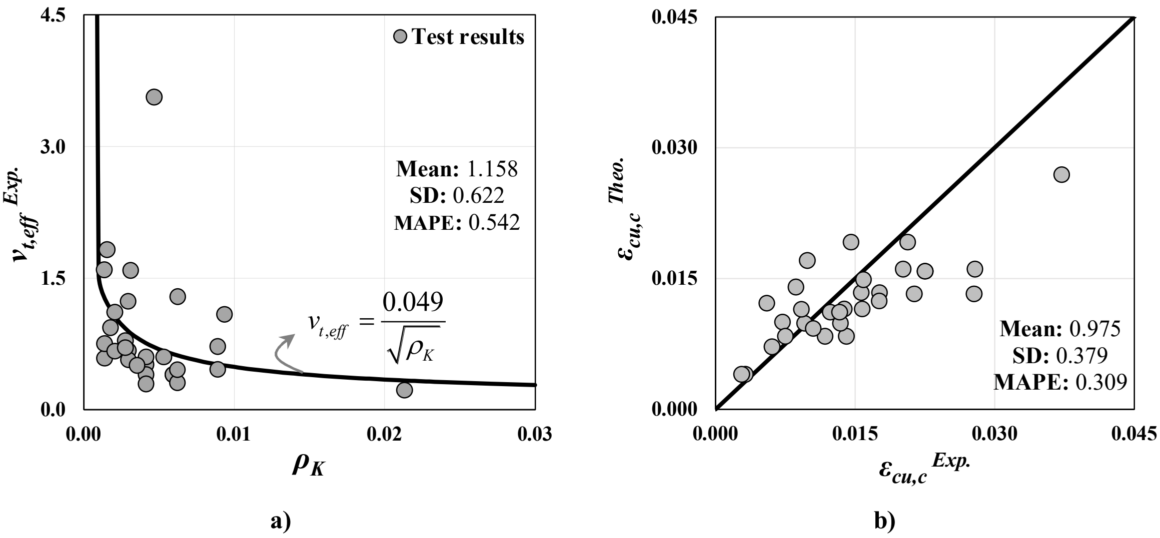

Fig. 15. Comparison between the experimental and theoretical results; a) $v_{t,eff}^{\text{Exp.}}$ vs ρ_K curve b) $\varepsilon_{cu,c}^{\text{Theo.}}$ vs $\varepsilon_{cu,c}^{\text{Exp.}}$ curve

Fig. 16

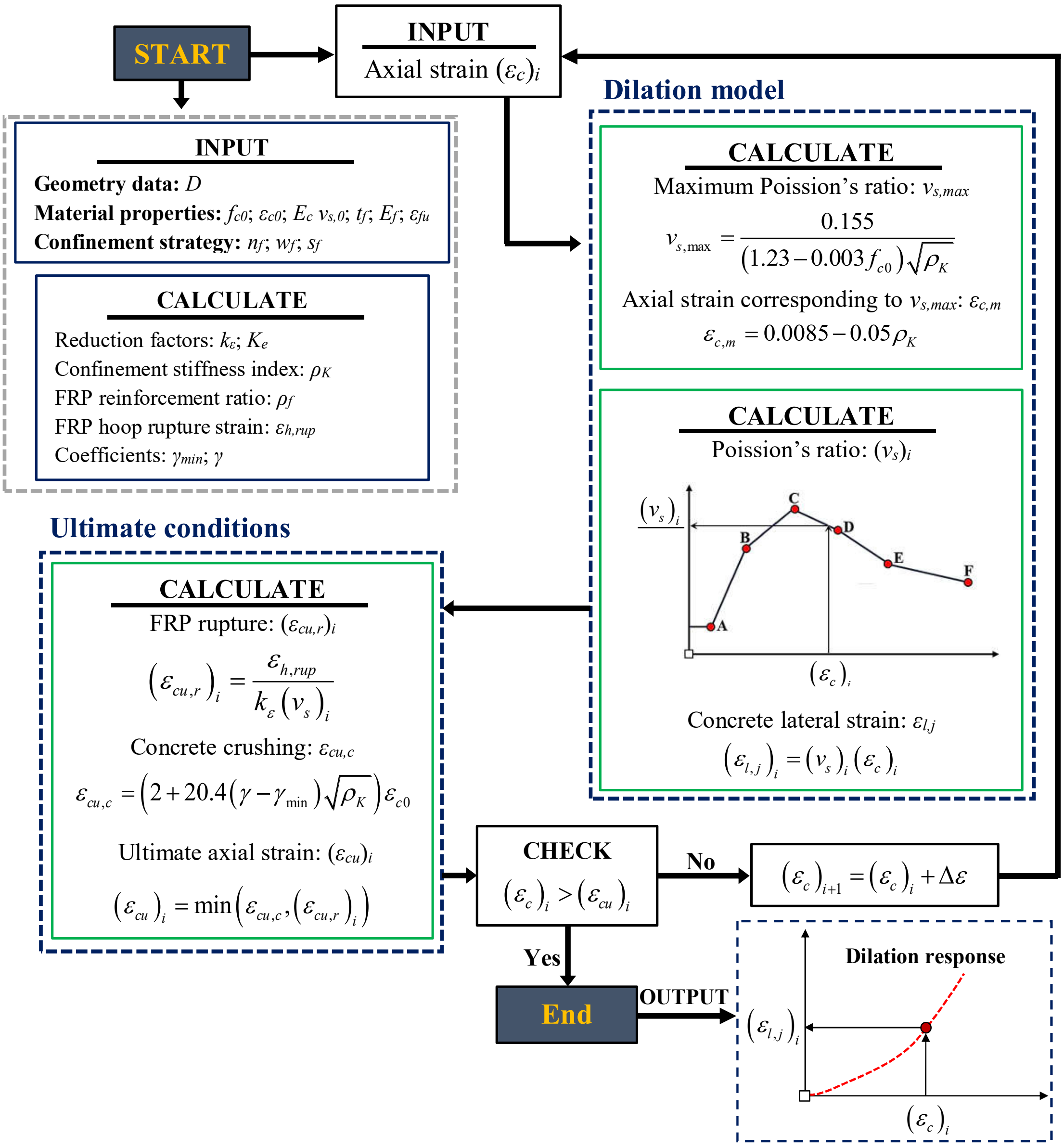

Fig. 16. A flowchart for calculating the dilation characteristics of FRP fully and partially confined concrete elements

Fig. 17

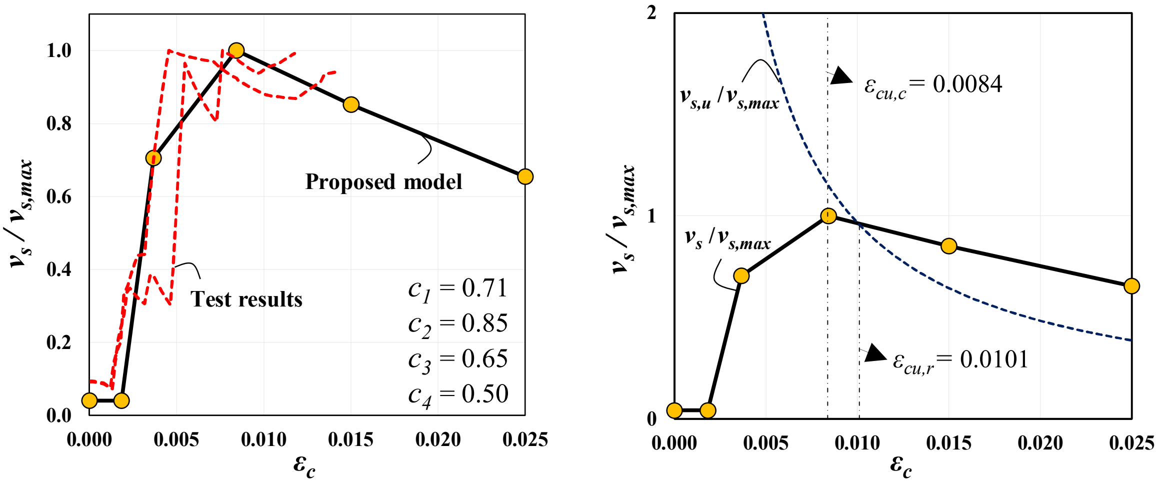

a) Dilation response b) Ultimate condition

Fig. 17. Determination of the dilation response of the test specimens of S-1-3-25 conducted by Zeng *et al.* (2018a) using the proposed model

Fig. 18

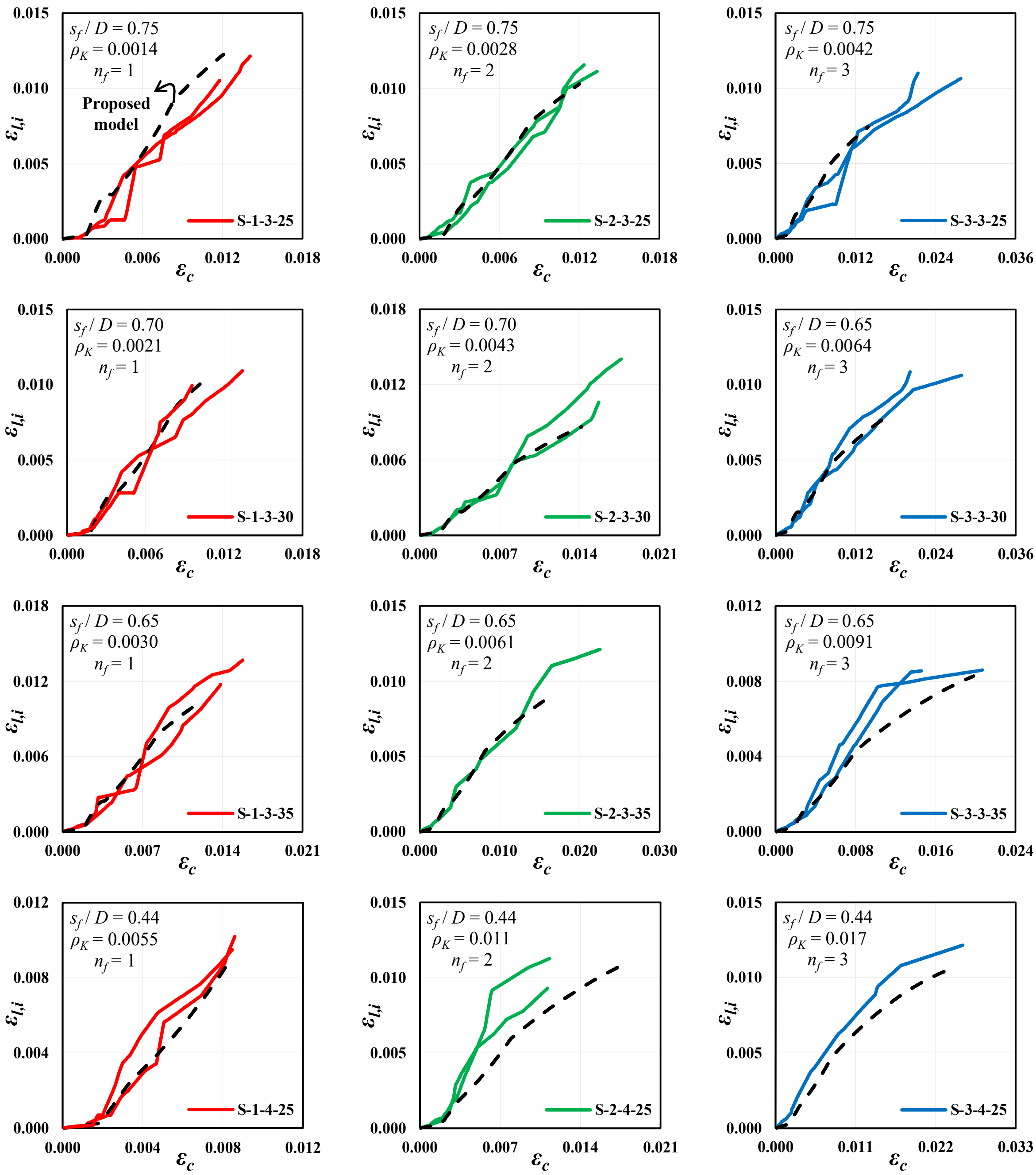
$s_f / D = 0.75$
$\rho_K = 0.0014$
$n_f = 1$
Proposed model
S-1-3-25
$s_f / D = 0.75$
$\rho_K = 0.0028$
$n_f = 2$
S-2-3-25
$s_f / D = 0.75$
$\rho_K = 0.0042$
$n_f = 3$
S-3-3-25
$s_f / D = 0.70$
$\rho_K = 0.0021$
$n_f = 1$
S-1-3-30
$s_f / D = 0.70$
$\rho_K = 0.0043$
$n_f = 2$
S-2-3-30
$s_f / D = 0.65$
$\rho_K = 0.0064$
$n_f = 3$
S-3-3-30
$s_f / D = 0.65$
$\rho_K = 0.0030$
$n_f = 1$
S-1-3-35
$s_f / D = 0.65$
$\rho_K = 0.0061$
$n_f = 2$
S-2-3-35
$s_f / D = 0.65$
$\rho_K = 0.0091$
$n_f = 3$
S-3-3-35
$s_f / D = 0.44$
$\rho_K = 0.0055$
$n_f = 1$
S-1-4-25
$s_f / D = 0.44$
$\rho_K = 0.011$
$n_f = 2$
S-2-4-25
$s_f / D = 0.44$
$\rho_K = 0.017$
$n_f = 3$
S-3-4-25
$\varepsilon_{l,i}$
ε_c

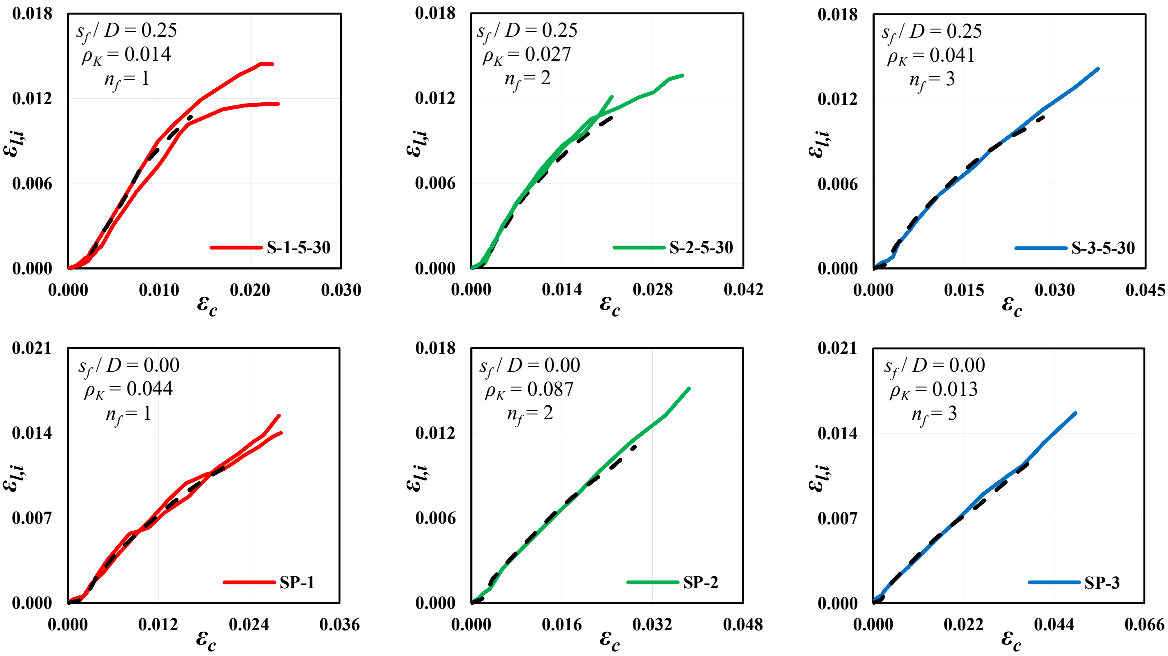

Fig. 18. Analytical analyses versus experimental results for the FRP fully and partially confined specimens tested by Zeng *et al.* (2018a)

Figure 19 Click here to access/download;Figure;Fig 19.pdf

Fig. 19

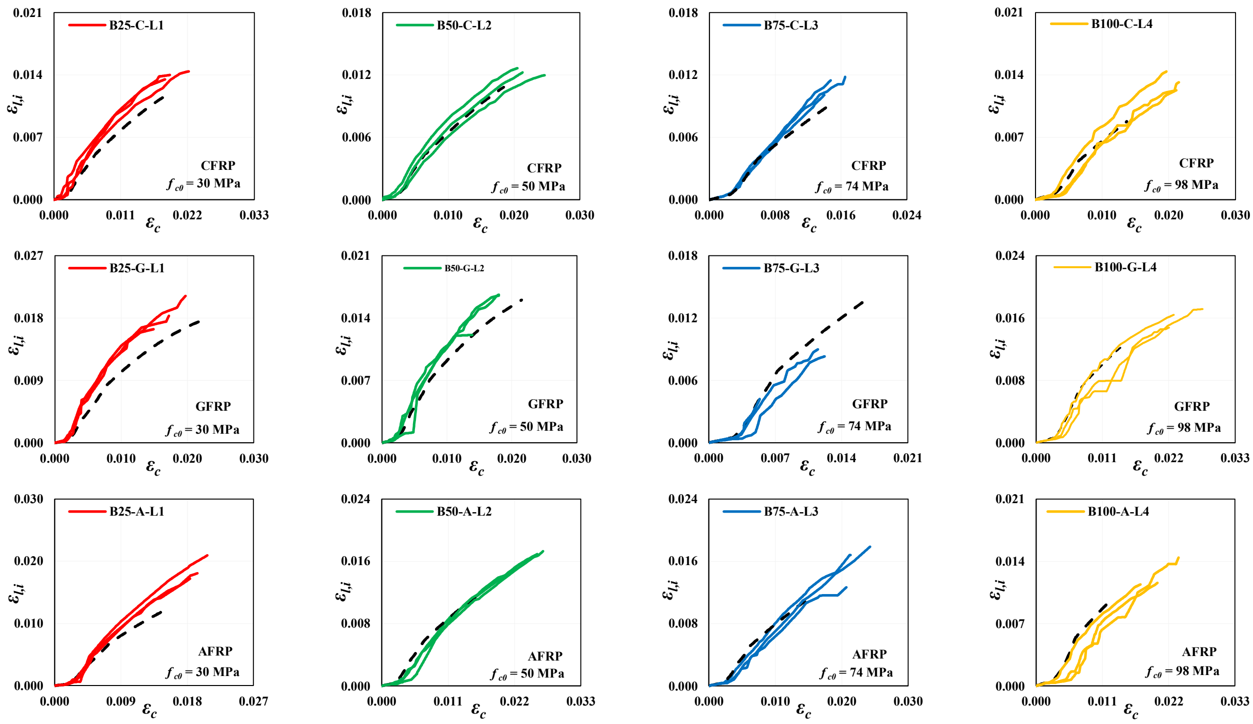

Fig. 19. Analytical analyses versus experimental results for the FRP fully confined specimens tested by Lim and Ozbakkaloglu (2014c)

Fig. 20

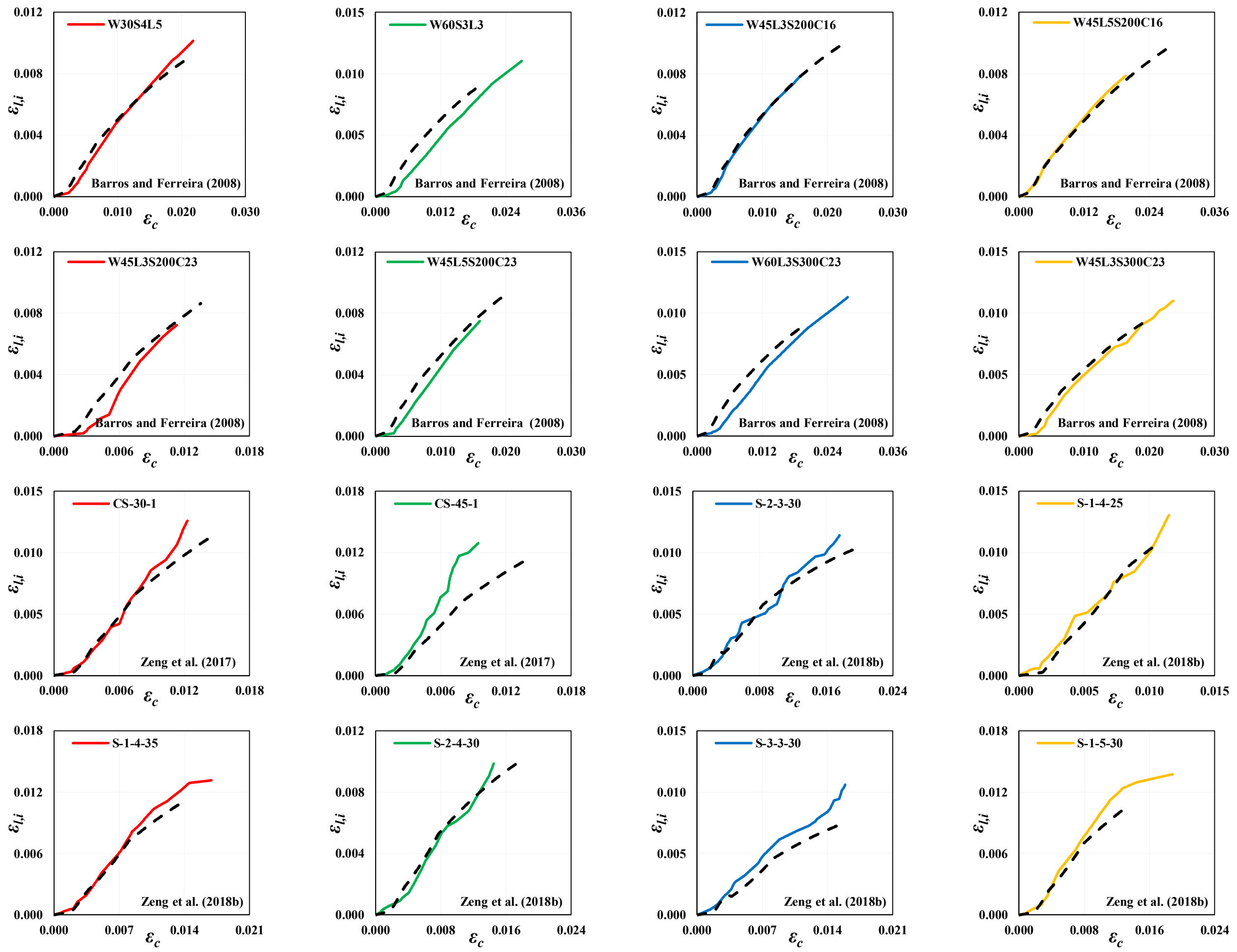

Fig. 20. Analytical analyses versus experimental results for the FRP partially confined specimens tested by Barros and Ferreira (2008), Zeng *et al*. (2017) and Zeng *et al*. (2018b)